Mission Design Aspects for the Mass Change and Geoscience International Constellation (MAGIC)

Betty Heller-Kaikov[1], Roland Pail[1] and Ilias Daras[2]

[1] *Chair of Astronomical and Physical Geodesy, Technical University of Munich (TUM), Arcisstraße 21, 80333 München, Germany.*
E-mail: betty.heller@tum.de
[2] *European Space Agency, Earth & Mission Science Division, ESTEC, Noordwijk, The Netherlands.*

This is a pre-copyedited, author-produced PDF of an article accepted for publication in Geophys. J. Int. following peer review. The version of record **B. Heller-Kaikov, R. Pail and I. Daras, Mission design aspects for the mass change and geoscience international constellation (MAGIC), Geophysical Journal International, Volume 235, Issue 1, October 2023, Pages 718–735, https://doi.org/10.1093/gji/ggad266** is available online at: `https://academic.oup.com/gji/advance-article-abstract/doi/10.1093/gji/ggad266/7218566?utm_source=advanceaccess&utm_campaign=gji&utm_medium=email`.

SUMMARY

The Mass Change and Geoscience International Constellation (MAGIC) is planned as the first realisation of a double-pair low-low satellite-to-satellite (ll-sst) tracking gravity mission consisting of a polar and an inclined satellite pair. Due to the much increased spatial and temporal resolution and multi-directionality of the data to be collected by this mission, new possibilities regarding the resolvability of mass transport processes in space and time are expected. In order to maximise the scientific and societal outcome of this mission, an optimisation of both the mission design as well as the methods to process the expected data is fundamental. Using numerical closed-loop simulations, we investigate the impact of several key mission design aspects on the gravity retrieval from a double-pair constellation such as the planned MAGIC mission. Specifically, we show how the choice of the second pair's inclination poses a trade-off between a reduction of retrieval errors at latitudes covered by data from both pairs and at higher latitudes, thereby requiring a compromise between the latitude-dependent accuracy requirements of different user groups. One of the key mission goals is to provide fast-track gravity products with short latency for operational service applications. Towards the estimation of such short-term gravity fields of a few days, we investigate if coordinating the polar and inclined pairs' orbits to achieve a stable ground-track coverage is necessary for obtaining a homogeneous accuracy of subsequent gravity solutions. Indeed, combining two freely drifting, uncontrolled orbits significantly degrades short-term gravity fields in time periods in which both pairs show coinciding ground track gaps. Finally, we analyse the relative performance of the two satellite pairs. Double-pair scenarios that are strongly dominated by the inclined pair's data reveal degraded gravity solutions when co-estimating daily gravity fields as de-aliasing strategy. This effect can be mitigated by choosing a more balanced double-pair configuration, e.g. by choosing similar orbit heights and instrument noise levels for both satellite pairs. The findings presented in our study will serve to optimise the system design of the upcoming MAGIC constellation.

Key words: Satellite gravity; Time variable gravity; global change from geodesy; satellite geodesy.

1 INTRODUCTION

Global observations of the temporal variations of the Earth's gravity field provide insight into geophysical processes that involve mass redistributions. Especially the data from the satellite gravity missions Gravity Recovery and Climate Experiment (GRACE, 2002-2017, (Tapley et al. 2004)) and its successor mission GRACE-Follow on (GRACE-FO, since 2018, (Flechtner et al. 2017), (Kornfeld et al. 2019)) had and still have an enormous impact on the qualitative and quantitative understanding of geophysical processes in the fields of continental hydrology (e.g. (Guentner 2008), (Schmidt et al. 2008), (Rodell et al. 2018)), glaciology (e.g. (Ramillien et al. 2006), (Luthcke et al. 2013), (Velicogna et al. 2014)), oceanography (e.g. (Peltier 2009), (Chambers et al. 2010)), atmosphere (e.g. (Forootan et al. 2014)) and solid Earth science (e.g. (Han et al. 2013), (Panet et al. 2014), (Panet et al. 2022)).

In addition to the scientific value of these data, observing the gravity field over time is also of societal relevance, e.g. to monitor climate change impact such as the melting of glaciers (e.g.

(Wouters et al. 2019)) and sea level rise (e.g. (Lombard et al. 2007), (Cazenave et al. 2009), (Ivins et al. 2013)), as well as groundwater depletion (e.g. (Taylor et al. 2013)), floods (e.g. (Chen et al. 2010), (Espinoza et al. 2013)) and droughts (e.g. (Frappart et al. 2012)).

As stated by (Pail et al. 2015), the science and user needs for gravity data both point to a continuation of the present temporal global gravity dataset, as well as to an improvement of the spatial (target: 100 km) and the temporal (target: 1 to a few days) resolution compared to GRACE and GRACE-FO which provide monthly to sub-monthly gravity fields down to 200-500 km spatial resolution. Challenges to provide continuous satellite gravity measurements for the next decades are the limitation of each mission's lifetime due to the required low (300-500 km) orbit heights, as well as the high costs for dedicated gravity missions.

Towards successor missions for GRACE-FO that meet the above-mentioned science and user needs, numerous studies have been performed (e.g. (Sharifi et al. 2007), (Sneeuw et al. 2008), (Wiese et al. 2009), (Wiese et al. 2012), (Elsaka et al. 2014), (Gruber et al. 2014), (Hauk and Pail 2019) and (Pail et al. 2019a)). These include simulations of single- and double-pair concepts involving various in-line (i.e., GRACE(-FO)-like) and pendulum configurations. The latter is a constellation of two satellites, whose orbits differ by their right-ascension and mean anomaly, resulting in a pendulum motion of the trailing satellite with respect to the leading satellite with a period of once per revolution. By this constellation, cross-track information is added to the pure in-line information of the GRACE concept. The degree of reduction of temporal aliasing effects is closely related to the opening angle of the pendulum.

Especially the realisation of a double-pair mission as described by (Bender et al. 2008) would not only allow to significantly reduce temporal aliasing errors, which are the main error contributor in GRACE and GRACE-FO fields ((Flechtner et al. 2016), (Visser et al. 2010), (Wiese et al. 2011a)), but also increase the temporal resolution of the derived fields. The latter would enable the application of processing concepts, such as near-real time processing (Purkhauser and Pail 2019) and the de-aliasing without the need of background models by co-estimating daily fields as described by (Wiese et al. 2011), in real data processing.

Double-pair constellations have been extensively studied at both ESA ((Iran Pour et al. 2015), (Daras and Pail 2017), (Dionisio et al. 2018), (Purkhauser et al. 2019), (Purkhauser et al. 2020), (Haagmans et al. 2020a), (Massotti et al. 2020)) and NASA ((Srinivasan et al. 2019), (Wiese and Hauk 2019), (Wiese et al. 2022)). Since 2011 ESA and NASA explore a possible cooperation on a future gravity mission under the umbrella of the Joint Programme Planning Group (JPPG), which was established between NASA and ESA for cooperation in the field of Earth Observation.

Arising from NASA's Mass Change Designated Observable (MCDO) and ESA's Next Generation Gravity Mission (NGGM) studies, the Mass Change and Geoscience International Constellation (MAGIC) is a double-pair mission concept for which a Mission Requirements Document (MRD) (MAGIC MRD, 2020) has been jointly developed and published by the two agencies. The MRD details the requirements of the various scientific user groups, which motivate the overall setup of the mission: MAGIC is planned to deliver at least 7 years of global observations and consist of one near-polar and one 65° to 70° inclined satellite pair, with orbits ensuring a near-homogeneous sampling over 5 to 7 days (MAGIC MRD, 2020). As such, the mission aims at continuing the gravity data time series given by the GRACE and GRACE-FO mission, as well as providing data of improved resolution and accuracy compared to the data currently available from GRACE and GRACE-FO. Additionally, a special focus is set on providing input for service applications such as flood early warning services, which especially require near real time (NRT) techniques to provide short-term gravity products with short latency.

Information on the instrumental design for MAGIC is given by (Massotti et al. 2021): The payload of the mission's satellites shall include a laser ranging interferometer (LRI) as main payload for measuring the inter-satellite distance, accelerometers measuring the non-gravitational accelerations, GNSS receivers and passive retroreflectors. As one of the aims of the mission is to provide short-term gravity fields of few days with homogeneous spatial resolution, an attitude and orbit control system is planned to be built at least in the inclined pair, keeping the satellites' orbit altitude and maintaining a homogeneous ground track pattern also for shorter gravity retrieval periods. While the polar pair will – in the current planning – use accelerometers of the so-called SuperSTAR class ((Frommknecht et al. 2003)), which are already payload of GRACE-FO, the inclined pair shall host a newly developed MicroSTAR instrument ((Cesare et al. 2022)), which has an improved performance by about one order of magnitude (cf. section 2.1.2).

The polar pair will be realised in the frame of NASA's MCDO as a joint effort of NASA and DLR (German Aerospace Center) with a target launch date in 2028. In the current planning, the initial altitude will be about 500 km, and decaying due to air drag, resulting in a drifting orbit similar to GRACE and GRACE-FO. The inclined ESA pair (NGGM) has a target launch date in 2031. According to the current baseline, it will have a coordinated repeat orbit with pre-defined sub-cycles in a constant altitude of about 400 km and an inclination of 70°. Together, the two pairs form the MAGIC constellation.

Working towards the realisation of this mission, on NASA side, a phase-A MCDO study was completed in 2022, and the next phases shall be kicked-off by mid 2023.

On ESA side, besides two parallel industry phase-A studies for NGGM/MAGIC, a science support study (TUM IAPG 2020) was carried out from spring 2021 to autumn 2022 (and is now continued to autumn 2023), in order to identify an optimum mission design in terms of orbits and instrument performance specifications as feedback to the parallel industry studies, and to investigate enhanced processing strategies for a double-pair mission such as MAGIC. These goals were achieved using end-to-end numerical closed-loop simulations in which the errors of the retrieved level 2 gravity fields can be computed, as the "true world" is perfectly known. Two independent full scale numerical simulators from TUM and GFZ have been validated against each other to provide very comparable results which are consistent with the accuracy demands of MAGIC gravity field products.

In our paper, we present selected results of the aforementioned ESA science support study. These involve quantifying the impact of central design parameters of the MAGIC mission on the accuracy of gravity field products derived from the data. For each of the considered design aspects, we specifically focus on parameter options that are within the range of what is currently considered for MAGIC. Of course, the final decision on mission design parameters is constrained by multiple factors such as, e.g., technical feasibility or cost (see e.g. (Wiese et al. 2022) for a comprehensive analysis of possible mission designs considering the scientific outcome, financing, risk, schedule and cooperation possibilities for a gravity mission succeeding GRACE-FO).

To relate the expected MAGIC double-pair performance to the currently available GRACE and GRACE-FO data, as well as place these performance levels in a larger context, we give an overview of a broader trade space of possible gravity mission configurations in section 3.1. These are various configuration concepts such as single- and double-pair missions, including satellite pairs with pendulum-like relative motion instead of the GRACE-type in-line formation.

Regarding the concrete mission design for MAGIC, we quantify the impact of the second satellite pair's inclination in section 3.2.1. This is done by comparing two possible mission scenarios representing the end members of the considered inclination range for the real MAGIC mission, i.e. 65° and 70°. The results show that the second pair's inclination represents an important mission design parameter involving a trade-off between complying with the (latitude-dependent) accuracy requirements given by different user communities.

As mentioned above, meeting the goal of a homogeneous data coverage within subsequent gravity retrieval intervals will require orbit control, keeping specific (time-discrete) subcycles of stable longitudinal shift (Massotti et al. 2021). Thereby, an orbit subcycle of a certain length provides a uniform ground track density for subsequent periods of time matching the subcycle length. As the wanted gravity retrieval period might depend on the specific scientific and/or service application, the question on the impact of a mis-match between subcycle length and retrieval period remains to be answered. In section 3.2.2, we evaluate this question based on a 3-day gravity retrieval using double-pair data collected from a 5-day subcycle orbit. The section also addresses the question if a coordination of the orbits of the polar and inclined pair is necessary for short-term gravity retrieval, or if it is sufficient to keep stable subcycles on the inclined pair, while the polar pair is freely drifting, similarly to the GRACE(-FO) setup.

One of the aims of the MAGIC mission is the better extraction of short- and long-period signals from the satellite data, which is facilitated by the higher temporal resolution of the double-pair data. Especially the separation of short-period atmospheric signals is one of the objectives formulated in the MRD. A method to co-estimate low-spherical harmonic (SH) degree daily gravity fields along with a multi-day higher-resolved field is presented in (Wiese et al. 2011). This method can be used as de-aliasing strategy for double-pair data processing, thereby representing an alternative to the model-based de-aliasing typically applied in GRACE(-FO) data processing. As shown by (Wiese et al. 2011) and (Abrykosov et al. 2022), applying the processing strategy presented in the former to GRACE(-FO)-type single-pair data does not provide a significant benefit as opposed to the case of a double-pair constellation of Bender type. In section 3.2.3, we show that the applicability of the (Wiese et al. 2011) processing method on the MAGIC double-pair data will depend on the mission design, specifically on the relative performance of the two satellite pairs, which makes the latter an important parameter to consider for the MAGIC mission design.

Our paper is structured as follows: Section 2 provides an overview of the used simulation framework and post-processing strategy. The results presented in section 3 include a comparison of various single- and double-pair scenarios in section 3.1 as well as analyses on the impact of MAGIC mission design parameters, being the second pair's inclination, the match between orbit subcycle length and retrieval period and the relative performance of the two satellite pairs, in section 3.2. Section 4 relates our findings to results found in previous studies, after which section 5 summarises the conclusions of our studies and gives an outlook.

2 DATA AND METHODS

2.1 Full-scale gravity simulations

2.1.1 Simulation environment and parametrisation

The closed-loop simulations are performed using the full-scale gravity simulation software at the Institute of Astronomical and Physical Geodesy (IAPG), which is described in detail in (Daras et al. 2015) and (Daras 2016). The included gravity retrieval method is based on the short-arc approach (Mayer-Gürr 2006). For the simulations of the present paper, an arc length of 6 h is used. A cross-validation with a second numerical simulator implementation at GFZ, which is based on the operational EPOS software and is using classical numerical integration, shows very similar results, demonstrating that the main conclusions derived from the simulation studies are independent of the used retrieval approach. A performance comparison of our simulation software with several Chinese gravity field groups using various gravity retrieval methods underlines this conclusion ((Pail et al. 2019b)).

In the following, we outline the main steps of the simulation procedure. The details on the used background models and specific noise assumptions applied for the simulations of the present paper are given in section 2.1.2.

In the forward computation step, orbits (i.e., position and velocity time series) of the satellites are computed at a sampling rate of 5 s. This is done by numerically solving the equations of motion of the satellites using a multi-step method according to (Shampine and Gordon 1975). As input for the orbit computation, the satellites' position and velocity vectors at initial time are required, which need to be computed in advance for the orbit to satisfy certain desired properties (for more details on the orbit parameters, see section 2.1.2 and Tab. 1). Moreover, the integration requires force models that describe the "true" static and time-variable gravity fields within the simulation.

Based on the simulated orbits, synthetic observations representing GNSS (Global Navigation Satellite System) positioning data (high-low satellite-to-satellite tracking observations, hl-sst) and inter-satellite distance data (low-low satellite-to-satellite tracking observations, ll-sst) are computed. To make these synthetic observations more realistic, instrument noise generated from assumed noise spectra is added.

For the following gravity inversion step which is based on the short-arc approach, residual hl-sst and ll-sst observations are computed. This involves computing reference observations at the positions along the before-computed (noise-free) orbit, using the integral formula given in (Mayer-Gürr 2006) and reference models for the static and temporal gravity field. At this stage, the accelerometer noise, treated as acceleration difference in the line-of-sight direction between the two satellites of a pair, is applied.

The normal equations (NEQ) are assembled based on the observation equations of the short-arc approach, involving both gravity field coefficients as well as orbit parameters as unknowns. The coloured stochastic noise as included in the residual observations is taken into account by applying appropriate stochastic models as weighting matrices. After adding the hl-sst and ll-sst NEQ systems representing data periods within the regarded retrieval period, the equation system is solved in a least-squares sense applying a standard Gauss-Markov model.

In the setup of the NEQs, we distinguish two processing schemes: In the nominal processing, one set of SH coefficients with maximum degree and order (d/o) N_{max} describing the mean gravity field within the retrieval period is estimated. For this processing scheme, an atmosphere and ocean de-aliasing (AOD) product is applied when computing the residual observations in order to reduce the temporal aliasing errors produced by high-frequency non-tidal AO signals which are not captured by the temporal sampling of the satellites.

As an alternative to the above-described model-based dealiasing, short-term signals, which would otherwise cause temporal aliasing, can be directly parametrised as described in (Wiese et al. 2011) by co-estimating low-SH degree daily gravity fields. The main idea of this approach is to extract as much high-frequency information from the data as possible, and thus parameterising signals which would otherwise alias into the longer-term solutions ((Wiese et al. 2011)). Beyond this 'self-dealiasing' aspect, short-term solutions result with short latency, which are expected to reflect reality better than a-priori geophysical models, and can be used for operational service applications, such as drought or flood monitoring and forecasting, or water management applications ((Pail et al. 2015), (Purkhauser and Pail 2019), (Massotti et al. 2021)).

In this processing scheme, for each day within the considered (multi-day) retrieval period, a separate set of SH parameters with maximum SH d/o of $N_{\mathrm{max,DWS}}$ (DWS: daily Wiese solutions) is parametrised, along with one set of SH coefficients for degrees $N_{\mathrm{max,DWS}} + 1$ to N_{max} describing the high-degree part of the mean field over the retrieval period. After solving the NEQ system containing all parameters, the DWS can be separately considered as long-wavelength daily fields. Additionally, the mean of the DWS coefficients is formed and combined with the larger-degree mean field for the retrieval period to have a full set of SH coefficients describing the mean field of the considered retrieval period. Of course, the temporal resolution in this processing scheme is restricted to 1 day, while sub-daily signals (such as typically ocean tides) can still not be captured. For this, an extended satellite constellation would be necessary ((Pfaffenzeller et al.2023)). Alternatively, also a hybrid strategy in which signals with periods shorter than the Nyquist period of 2 days are reduced by means of external models, and the rest is captured by the DWS would be possible.

2.1.2 Background models and noise assumptions

This section gives an overview on the models and assumptions used in the full-scale simulations for the present paper. All simulations refer to the period of time starting on January 1st, 2002. Depending on the specific analysis, we compute monthly (31 days), weekly (7 days) or short-term (3 days) solutions. NEQs are assembled and solved up to a maximum SH d/o of 120, 100 or 70, depending on the retrieval period. This means we select the maximum possible d/o allowed by the ground track density in the respective retrieval time interval, in order to avoid spectral leakage of larger-degree signal components to the lower-degree SH coefficients of the solution due to under-parameterisation.

The orbit scenarios underlying the simulations are summarised in Tab. 1, where the identifier given in the second column is used in the following to refer to the individual orbits. For all simulations in the present paper, an inter-satellite distance of 220 km between the two satellites of a pair is assumed.

The orbit selection procedure, described in detail in (Massotti et al. 2021), is optimised to achieve particular orbit subcycles (for which reason most orbit scenarios in Tab. 1 differ by more than one of the shown parameters). For example, in the 3d_H orbit scenario, the satellites approximately arrive back at their initial (Earth-fixed) position after 3 days, with a westward shift of about 3° which is coordinated between the two satellite pairs, such that the double-pair ground track pattern in subsequent 3-day periods is exactly the same. (This is the ideal scenario which maximises ground track homogeneity over time.)

For MAGIC, orbits with both sub-weekly as well as monthly subcycles are aimed for, following the user requirement of a sustained homogeneous spatial sampling at multiple temporal resolutions/retrieval periods. The requirement is needed in order to be able to resolve geophysical processes taking place on multiple time scales.

Keeping the satellites in such an orbit can only become practically realised if a drag compensation system and an attitude and orbit control is in place. This is a difference to the predecessor missions GRACE and GRACE-FO, which – besides occasional orbit maneuvers – are left freely drifting. This has a negative effect on the gravity performance especially in certain periods where the orbits experience deep resonances, i.e. very short repeat cycles (e.g. (Wagner et al. 2006)). Since MAGIC is dedicated to provide inputs for operational service applications are planned, a consistent quality of subsequent gravity data products is required, and therefore an orbit control system is planned to be implemented ((Massotti et al. 2021)).

The required level of strictness of the orbit control for MAGIC is tested in 3.2.2, where the necessity of an orbit coordination between the two satellite pairs is tested in view of short-term solutions.

In terms of background models, for the forward modeling (i.e., the computation of synthetic observations, see section 2.1.1) we use the static gravity field model GOCO05s (Mayer-Gürr et al. 2015), the ocean tide model EOT11a (Savcenko and Bosch 2012) and the full atmosphere, ocean, hydrology, ice and solid Earth (AOHIS) signal given by the updated Earth System Model of ESA (Dobslaw et al. 2015). The latter gives realistic temporal gravity variations at a temporal resolution of 6 h.

For the computation of reference observations in order to compute residual observations, the same static model is used, assuming no errors of this model. This assumption is reasonable as errors in the static background model produce much smaller gravity retrieval errors compared to error sources such as the ll-sst ranging noise or temporal aliasing errors, as shown by (Flechtner et al. 2016).

As reference ocean tide model, GOT4.7 (Ray 2008) is applied, meaning that we use the difference of the two ocean tide models EOT11a and GOT4.7 as a measure for the ocean tide background model error. In the case of the nominal processing scheme (see section 2.1.1), the AOD product, along with an error estimation of it, as given by (Dobslaw et al. 2016), is used in the inversion, such that HIS signals are retrieved. In the case of a co-estimation of low-resolved daily gravity field models according to (Wiese et al. 2011), no AOD product is applied, such that AOHIS signals are retrieved. This is done with the intention to present results of two independent de-aliasing strategies for double-pair data, one purely background model-driven and one purely data-driven. In general, all background models are used up to d/o 120.

In terms of instrument noise assumptions, for the hl-sst observations, a 1 cm white noise for 3-d positions is assumed to take into account the sensor noise for the GNSS observations. Since the impact of orbit errors is much lower than the dominant instrument errors related to ACC and LRI, this simplifying assumption can be justified. However, we plan to include a coloured noise model also for orbit errors in future work.

As full drag compensation is assumed, no non-gravitational signals measured by the accelerometer instruments are modeled in

Table 1. Double-pair orbit scenarios used for the simulations in the present paper. The IDs are consistent to (Massotti et al. 2021) and give information on the subcycle length in days and the altitude (L for low, M for mid, H for high orbits). Scenarios in which the polar and the inclined pair's orbit subcycles or longitudinal drifts per subcycle differ have IDs starting with the letter U, standing for "uncoordinated". Mean altitude, inclination and longitudinal shift per subcycle $\Delta\lambda_{\text{shift}}$ are specified for the polar and inclined pair's orbits for each of the scenarios.

description	orbit ID	altitude/km	inclination/°	$\Delta\lambda_{\text{shift}}$/°	subcycles/days
3-day subcycles, high altitude	3d_H	463 432	89 70	-3.067 (3d) -3.076 (3d)	3, 7, 31
5-day subcycles, mid altitude (65°)	5d_Ma	434 396	89 65	-1.458 (5d) -1.499 (5d)	2, 3, 5, 13, 18, 31
5-day subcycles, mid altitude (70°)	5d_Mb	425 397	87 70	0.733 (5d) 0.736 (5d)	2, 5, 27, 32
uncoord. 3-/5-day subcycles high altitude	U3d5d_H	492 432	89 70	-0.790 (5d) -3.076 (3d)	5, 31 3, 31
uncoord. 5-day subcycles, high altitude	U5d_H	492 460	89 70	-0.790 (5d) -0.284 (5d)	5, 31 5
uncoord. 3-day subcycles, high altitude	U3d_H	463 402	89 65	-3.067 (3d) 2.380 (3d)	3, 7, 31 3, 29-30
5-day subcycles, low altitude	5d_LL	376 344	89 70	-1.628 (5d) -1.671 (5d)	1, 2, 5, 12, 29
5-day subcycles, high/low altitude	5d_LH	492 344	89 71.5	-0.790 (5d) -0.732 (5d)	5, 31 5, 32

our simulations. The non-perfectness in the drag compensation is taken into account using models for the coloured noise of the accelerometers. Hereby, we distinguish two cases: A GRACE-type accelerometer with noise acc_G, approximating the performance of a SuperSTAR accelerometer (Frommknecht et al. 2003) and a NGGM-type accelerometer with noise acc_N, approximating the performance of a MicroSTAR accelerometer ((Lenoir et al. 2011), (Cesare et al. 2022)). The coloured noise of the accelerometers is described by the amplitude spectral densities

$$acc_{G,xyz} = 10^{-10}\sqrt{1 + \frac{0.005Hz}{f}}\frac{m}{s^2/\sqrt{Hz}}\,, \tag{1}$$

which expresses the GRACE-type accelerometer noise on each single accelerometer axis in each satellite and

$$acc_{N,los} = 10^{-11} \cdot \sqrt{\frac{\left(\frac{10^{-3}Hz}{f}\right)^2}{\left(\frac{10^{-5}Hz}{f}\right)^2 + 1} + 1 + \left(\frac{f}{10^{-1}Hz}\right)^4}\frac{m}{s^2/\sqrt{Hz}}\,, \tag{2}$$

which expresses the NGGM-type accelerometer noise as difference of the accelerometer measurements of the two satellites of a pair along their line of sight.

For the coloured noise of the laser ranging interferometer (LRI), which is assumed to be the ranging instrument for both satellite pairs of the MAGIC double-pair configuration, an amplitude spectral density that has been empirically derived from GRACE-FO has been used:

$$lri = 1.5 \cdot 10^{-9} \cdot \sqrt{\left(\left(\frac{0.028Hz}{f}\right)^3 + 1\right) \cdot \frac{\left(\frac{0.02Hz}{f}\right)}{\left(\left(\frac{0.00115Hz}{f}\right)^4 + 1\right)}}\frac{m}{\sqrt{Hz}}\,. \tag{3}$$

Depending on the processing scheme (nominal or daily coparameterisation), the retrieval error $\Delta x = x - x_{\text{(AO)HIS}}$ characterising the gravity retrieval performance of the considered simulated mission setup is computed as the difference of the retrieved SH coefficients x and the SH coefficients $x_{\text{(AO)HIS}}$ of the underlying "true" mean HIS or AOHIS signal of the respective period of time. This retrieval error includes the impact of the orbit geometry, the instrument measurement errors and temporal aliasing errors due to ocean tide and AOD background model errors. In contrast, the formal errors of the retrieved gravity coefficients, as computed based on the covariance matrix resulting from the parameter estimation procedure described in section 2.1.1, are independent of the (residual) observations and thus represent the impact of orbit geometry and instrument errors only.

In order to visualise and compare the global retrieval performance of several scenarios, we compute the degree amplitudes of their retrieval errors Δc_{nm} and Δs_{nm} in units of cm equivalent water height (EWH, (Wahr et al. 1998), (Schrama et al. 2007)) according to

$$\text{degr. ampl.}(n) = \frac{a\rho_e}{3\rho_w}\frac{2n+1}{1+k_n}\sqrt{\sum_{m=0}^{n}(\Delta c_{nm}^2 + \Delta s_{nm}^2)}\,, \quad (4)$$

where a is the semi-major axis of the Earth ellipsoid, ρ_e the mean density of Earth, ρ_w the density of water, k_n are the Love numbers, and n and m represent the SH degree and order.

In this paper, we consider single- and double-pair configurations of satellites flying in in-line or pendulum formations, with varying combinations regarding the accelerometer noise of the two satellite pairs. Except from section 3.1, which considers a broader trade space of possible mission configurations, our analysis concentrates on the following two double in-line pair scenarios:

(i) *Scenario 1:* one near-polar pair with a GRACE-type accelerometer (acc_G) + one inclined pair with a NGGM-type accelerometer (acc_N)
(ii) *Scenario 2:* one near-polar pair and one inclined pair, both with NGGM-type accelerometers (acc_N).

2.2 VADER filtering

Compared to the single-pair gravity solutions from the GRACE and GRACE-FO missions, the double-pair results from the MAGIC mission will show a very different spatial error characteristics. In order to evaluate the effect of post-processing on double-pair gravity retrieval errors in the framework of this manuscript, we therefore apply a filter that takes into account the specific error characteristics of each individual scenario by construction. The latter is achieved by building the filter on the full variance-covariance information of the considered gravity solution. Introduced by (Horvath et al. 2018), the VADER filter is defined as:

$$x_\alpha = (N + \alpha M)^{-1} N x = W_\alpha x\,, \quad (5)$$

where x and x_α are vectors containing the unfiltered and filtered retrieved SH coefficients, respectively. N is the NEQ matrix $A^T PA$ (with A being the design matrix and P being the weighting matrix), which is equal to the inverse of the retrieval error variance-covariance matrix. M is the inverse of the signal variance matrix, α is the scaling factor and W_α is the filter matrix. The matrix M is a diagonal matrix containing the reciprocal squares of the SH coefficients of the "true" monthly HIS signal. The value of α is determined as to minimise the root mean square (RMS) of the global error grid of the filtered model. As indicated by Eq. 5, the VADER filter is constructed based on the (co)variances of the considered solution x and thereby tailored to the solution's specific error structure.

The error Δx_α of the VADER-filtered gravity field solution x_α is computed as its difference to the (unfiltered) reference signal x_{HIS}:

$$\begin{aligned}\Delta x_\alpha &= x_\alpha - x_{\text{HIS}}\\ &= W_\alpha x - x_{\text{HIS}}\\ &= W_\alpha(x_{\text{HIS}} + \Delta x) - x_{\text{HIS}}\\ &= W_\alpha \Delta x + (W_\alpha - 1)x_{\text{HIS}}\,.\end{aligned} \quad (6)$$

As shown by Eq. 6, Δx_α consists of two parts: The filtered retrieval error $W_\alpha \Delta x$ and the HIS signal dampening $(W_\alpha - 1)x_{\text{HIS}}$. Applying a stronger (i.e. more strongly dampening) filter W_α leads to a decrease of $|W_\alpha \Delta x|$, as the error part contained in the retrieved field is increasingly dampened, but also to an increase of $|(W_\alpha - 1)x_{\text{HIS}}|$, as also the HIS signal part contained in the retrieved field is increasingly dampened.

Equation 5 shows that the filter strength depends on both the error (co)variances of the unfiltered solution x, which are represented by N, as well as on the determined value for α: For a fixed value of α, a gravity solution $x^{(1)}$ with larger retrieval errors and therefore larger error variances contained in N^{-1}, leads to a stronger filter W_α compared to a lower-error solution $x^{(2)}$. Likewise, for a fixed gravity solution x, choosing a larger value for α leads to a stronger filter compared to smaller values of α. As described above, the value of α is determined as to minimise Δx_α globally in a RMS sense.

Considering geophysical applications of the data, the above-described signal dampening introduced by the filtering is especially problematic, as it removes valuable signal information from the data. Any gravity mission design that requires weaker filtering is favorable. A quantification of the VADER filter impact on a single vs. a double-pair solution is given in section 6.1 in the appendix.

3 RESULTS

3.1 The choice of a double in-line pair configuration for MAGIC

Before presenting results on mission design parameters currently under investigation in the concrete planning of the MAGIC mission in the following section 3.2, we motivate briefly why a double in-line pair configuration of Bender type (cf. (Bender et al. 2008)), is chosen to be implemented for the MAGIC mission. To this end, we compare the closed-loop retrieval errors of several single- and double-pair configurations of in-line or pendulum pairs of satellites with varying combinations of accelerometer noise assumptions. The 11 studied scenarios are listed in the legend in Fig. 1. For all scenarios, 3d_H orbits as defined by Tab. 1 are used and two subsequent 31-day solutions are computed for each of the scenarios. The retrieval period of 31 days is chosen here to relate the different mission scenarios in terms of the standard level 2 monthly data products computed from data of the GRACE and GRACE-FO missions.

Figure 1 shows the retrieval errors computed as difference of the retrieved gravity coefficients to the reference HIS signal (left panel) as well as the formal errors extracted from the error variance-covariance matrix of the least-squares inversion (right panel), both in terms of degree error amplitudes (cf. Eq. 4). Each of the shown curves represents the mean of two degree error amplitude curves corresponding to the two subsequent 31-day solutions.

By comparing the error levels of the 11 scenarios in Fig. 1, we observe that double-pair configurations composed of a near-polar and a 70° inclined pair perform about one order of magnitude better than single pairs, which is due to the better sampling and observation geometry of the double-pair scenarios.

Comparing the in-line and pendulum single-pair scenarios in Fig. 1 shows that if full signal and noise retrieval errors are considered (left panel), the benefit of the multi-directional observations of pendulum formations determines the relative performance of the scenarios, while the replacement of the GRACE-type accelerometer by the NGGM-type accelerometer plays a minor role. This is due to the dominance of the temporal aliasing errors in the full

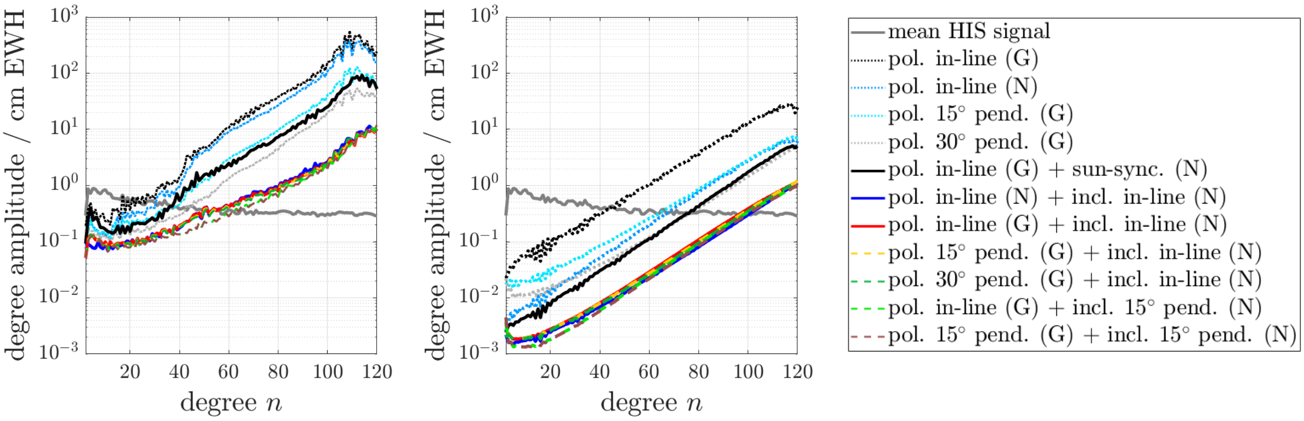

Figure 1. Degree error amplitudes of 31-day full signal and noise simulations for single- and double-pair scenarios based on 3d_H orbits (cf. Tab. 1). The left panel shows the HIS retrieval errors computed as difference of the retrieved signal and the HIS reference signal. The middle panel shows the formal errors of the inversion. As denoted in the legend, the dotted curves represent single polar pair scenarios, the solid curves double in-line pair scenarios composed of a polar (pol.) and an inclined (incl., inclination = 70°) or sun-synchronous (sun-sync., inclination = 97°) pair, and the dashed curves double-pair scenarios including one or two pendulum (pend.) pairs with opening angle of 15 or 30°, respectively. G and N represent the GRACE-type or NGGM-type accelerometer noise assumed, as defined in equations (1) and (2), respectively.

retrieval error budget, which can be significantly reduced by an enhanced observation geometry. In contrast, when considering formal errors (right panel) which only represent the impact of the spatial sampling and instrument errors and do not include temporal aliasing errors, the impact of the chosen accelerometer shows up more distinctly. Consequently, in order to fully exploit the benefit of an improved accelerometer for the gravity retrieval, the current level of temporal aliasing errors needs to be reduced significantly.

All considered double-pair scenarios (except from the one involving the sun-synchronous pair) included in Fig. 1 show very similar error levels. That is, using in-line or pendulum pairs in a double-pair configuration has no significant impact on the performance of the mission. This justifies the realisation of two in-line pairs as the MAGIC mission, also as they are cheaper and easier to implement than pendulum pairs.

The only double-pair scenario showing retrieval errors similar to the single-pair scenarios is the combination of a polar and a sun-synchronous pair, in which the inclination difference of the two pairs' orbits merely amounts to about 7°, compared to the 20° inclination difference between the polar and inclined orbital planes for the other double-pair scenarios. This shows that a rather low inclination of the second pair is crucial for the de-aliasing performance of a double-pair configuration. The trade-off between the needed low inclination of the second pair and the thereby implied polar gaps in the inclined pair's ground track is evaluated in section 3.2.1.

To summarise, our analysis of various combinations of in-line and pendulum pairs with differing accelerometer noise assumptions revealed that if the orbit altitude of the satellites is the same between the considered scenarios, the best global performance is achieved by using two satellite pairs of rather large (20°) inclination difference. Of course, double-pair missions also provide additional benefits such as the larger temporal resolution of the data, allowing for near-real time applications and short-term gravity retrieval. Mission design aspects regarding the performance of double in-line pair data for short-term gravity retrieval are presented in sections 3.2.2 and 3.2.3.

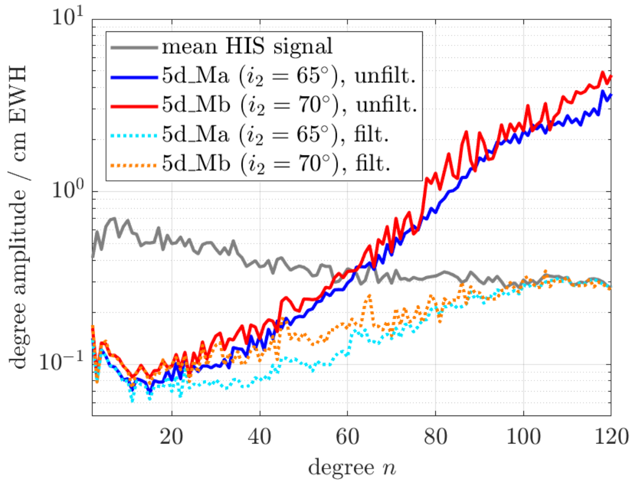

Figure 2. Degree error amplitudes of 31-day full signal and noise simulations for the Bender-type *scenario 1*, combining a polar in-line pair with GRACE-type noise and an inclined in-line pair with NGGM-type noise (cf. Eqs. (1) and (2)) based on 5d_Ma and 5d_Mb orbits (cf. Tab. 1), respectively. The blue and red solid curves (light blue and orange dotted curves) show the errors of the unfiltered (VADER-filtered) solutions.

3.2 Mission design aspects of MAGIC

3.2.1 Inclination of the second pair

In this section, the impact of the inclination of the second pair in a double-pair constellation on the gravity retrieval errors is analysed. To this end, we consider the double in-line pair *scenario 1* as defined at the end of section 2.1.2, and use the orbit scenarios 5d_Ma and 5d_Mb (cf. Tab. 1), in which the inclination of the second pair amounts to 65° and 70°, respectively. These two inclination values represent the endmember cases for the inclined pair to be implemented for the MAGIC mission, as stated in the MAGIC MRD (MAGIC MRD, 2020).

As shown by Tab. 1, the mean orbit altitude of the satellites is very similar between the two orbit scenarios, such that differences

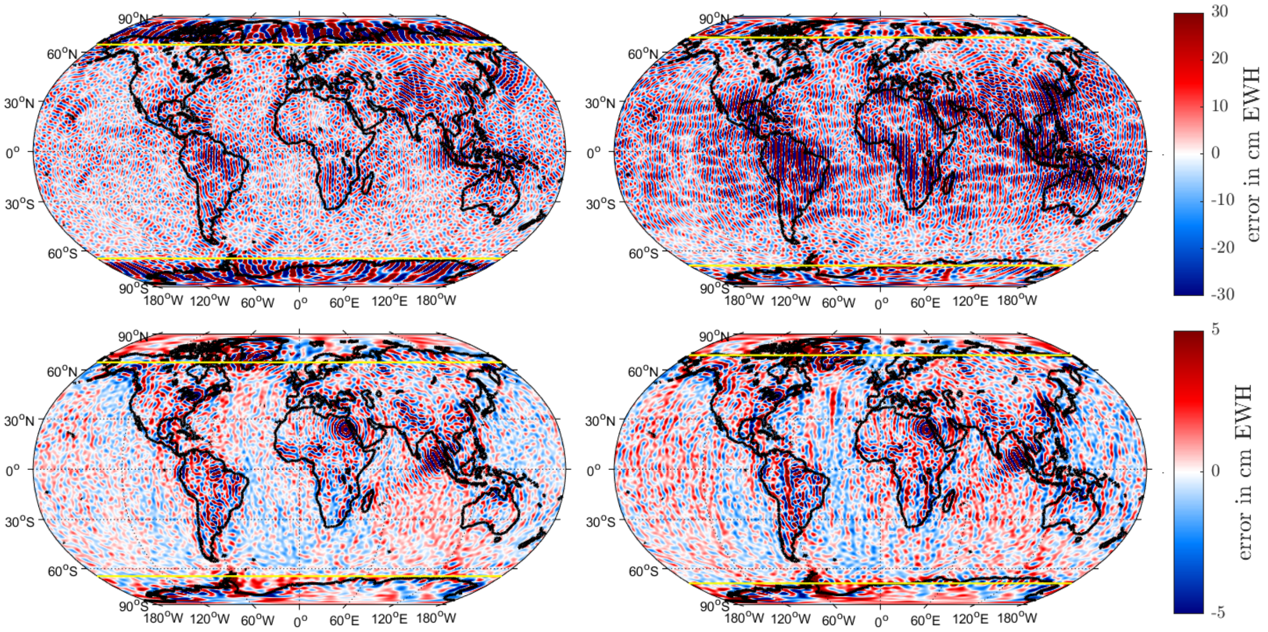

Figure 3. Retrieval errors of full signal and noise simulations for the same scenarios as in Fig. 2. The yellow lines in the left (right) panels mark the 65° (70°) inclination of the second satellite pair in the used 5d_Ma (5d_Mb) orbits (cf. Tab. 1) The top (bottom) panels show the errors of the unfiltered (VADER-filtered) solutions. Panels of the same row use the same colorbar.

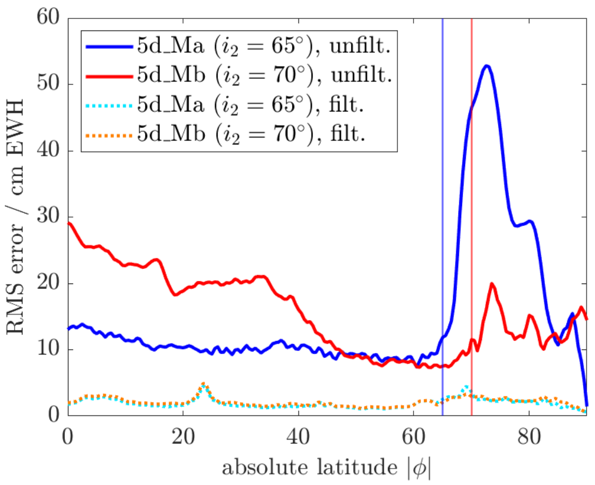

Figure 4. Root mean square values of the EWH error grid values shown by Fig. 3 computed along parallels (combining the grid values on the northern and southern hemisphere in one sum of squares), plotted as a function of absolute latitude, such that the average variation of the errors from the equator to the poles can be investigated. Shown are the errors of the unfiltered (blue, red) and VADER-filtered (light blue, orange) solution for the 31-day full signal and noise simulation of the same scenarios as in Figs. 2 and 3. The blue (red) vertical lines mark the 65° (70°) inclination of the second satellite pair in the used 5d_Ma (5d_Mb) orbits (cf. Tab. 1).

in the retrieval performance of the two scenarios can be interpreted as being caused almost exclusively by the different inclinations of the satellites of the second pair.

For both scenarios, we compute one d/o 120 31-day solution and compare their global performance by plotting the degree amplitudes of their retrieval errors in Fig. 2 as the blue and red curve. Despite the choice of demonstrating the impact of the second pair's inclination on the example of a single monthly solution, the qualitative results of the analysis are representative also for solutions of different temporal resolutions or periods of time.

In Figure 2 it is visible that, although the 65° scenario seems to outperform the 70° scenario, there are also intersections of the curves which indicate that the relative performance of the two investigated scenarios is not the same across the complete SH spectrum.

Comparing the spatial error patterns of the two scenarios in Fig. 3 (top panels) shows that a lower inclination of the second pair reduces the longitudinal striping noise in the latitude band in which both satellite pairs observe, visualising a better constraint on the sectorial SH coefficients of the gravity field. However, this is achieved at the cost of larger polar regions in which the double-pair performance is mainly given by the performance of the single polar pair. These observations indicate that there is a trade-off between the global error levels and striping reduction at lower latitudes and the size of the polar gaps of the inclined pair's orbit. This is also visualised in Fig. 4 where the latitude-dependency of the two scenarios' retrieval errors is compared.

In addition to the above-made analysis based on unfiltered solutions, in the following, the effect of post-processing on the relative performance of the two scenarios is investigated. For this purpose, for each of the two scenarios, a VADER filter as introduced in section 2.2 is constructed based on the NEQ matrix of the respective solution and applied to it.

As can be seen by considering the light blue and orange curves in Fig. 2 and 4 as well as the bottom panels of Fig. 3, the post-processing reduces the errors especially towards larger SH degrees and reduces the absolute performance difference between the two scenarios. As the VADER filter is specifically tailored to the error structure of the individual solution, it acts more strongly (i.e., causes a stronger dampening) at coefficients/in spatial regions where the errors in the considered solution are larger. Therefore, although the more similar performance of the two scenarios after the post-processing suggests that the impact of the second pair's inclination is not really important, it has to be noted that a smaller need for applying filtering is an important argument in favor of a specific mission design. This is emphasised by Eq. 6 which shows that a stronger filter does not only dampen the error but also signal components of the retrieved solution.

In the present case, both the lower errors in the regions covered by both pairs as well as the required weaker filtering speak in favor of choosing the lower (65°) inclination for the second pair such as given in scenario 5d_Ma. However, the better global homogeneity of the errors and the lower error levels in the polar regions where the data is used for research on the cryosphere speak for choosing the higher inclination of 70° such as given in scenario 5d_Mb. These conclusions show that the choice of the inclination of the second pair in a double-pair configuration will be a compromise, and depends on the latitude-dependent accuracy requirements that the scientific user groups of these double-pair data may have.

3.2.2 *Coordination of the polar and inclined orbits*

In this section, we assess the necessity of coordinating the orbits of the two satellite pairs of the MAGIC constellation in the context of short-term gravity retrieval of few days, in order to derive fast-track products with homogeneous quality for operational service applications. An orbit coordination provides a near-homogeneous sampling at constellation level. This is achieved at satellite-pair level by orbit control or orbit maintenance of each pair such that stable orbit subcycles at a common drift rate between the polar and inclined pair can be maintained.

For this analysis, a retrieval period of 3 days is chosen, as the maintenance of specific subcycles matching the desired retrieval period starts to become important when considering short-term gravity fields. For shorter time periods, the ground track density is naturally rather low such that deviations from a homogeneous data sampling have a larger impact on the gravity solutions.

In the following, we analyse the impact of two different aspects concerning the orbit coordination: Firstly, we test the necessity of maintaining 3-day orbit subcycles for both pairs in the case of 3-day gravity retrieval. Secondly, we test if, in the case of 3-day subcycles, a match of the drift rates between the two pairs is necessary.

In order to simulate several coordinated and uncoordinated cases in terms of orbit evolution and common subcycles between the two pairs, we consider the orbit scenarios 3d_H, U3d5d_H, U5d_H and U3d_H (cf. Tab. 1). 3d_H represents the ideal case, where our retrieval period of 3 days matches the common subcycle of both pairs and the orbits are coordinated to have a common drift, guaranteeing a stable ground track pattern in subsequent 3-day periods of time. As representative of the case where one pair in a free-drifting orbit is combined with another pair in a controlled orbit, U3d5d_H is chosen, as due to the missing 3-day subcycle of the polar pair, gaps in the 3-day ground track of the polar pair are resulting, which could similarly occur for a free-drifting polar pair. Furthermore, the case of two free-drifting satellite pairs is simulated by considering U5d_H in which the 3-day subcycle, which would guarantee a homogeneous 3-day ground track coverage, is missing for both pairs and the extreme case of coinciding gaps of the 3-day ground tracks of both pairs is realised. Such a condition could appear from time to time if both satellite pairs of the MAGIC configuration would be left free-drifting, without applying a specific orbit control. A relative comparison between these 3 cases demonstrates the impact of coordinating or controlling the orbits.

As mentioned above, our analysis on the coordination of the satellite orbits focuses on short-term gravity retrieval. For weekly to monthly gravity retrieval based on orbits used in the framework of this manuscript (cf. Tab. 1), a mismatch between the retrieval period and the exact orbital subcycle lengths present for the respective orbit does not impact the solutions significantly. This is due to the fact that all candidate orbits for MAGIC have close-to-weekly and close-to-monthly subcycles both with slight longitudinal shifts, leading to a sufficiently good data coverage to compute d/o 120 weekly and monthly double-pair solutions. In fact, investigations (not shown in this paper) revealed a scaling of the retrieval errors between weekly and monthly solutions according to the retrieval period, independently of the exact close-to-weekly and close-to-monthly subcycle lengths of the underlying orbits.

Figure 5 shows the 3-day ground tracks of the investigated orbit scenarios. The 3-day ground tracks of satellite pairs having a 5-day subcycle exhibit gaps that increase in spatial extent towards the equator. In the U3d5d_H orbits, the gaps in the polar pair's ground track are partly filled with data from the inclined pair, which is in contrast to U5d_H where the ground track gaps of both pairs coincide.

Figure 6 shows the degree error amplitude curves averaged over five subsequent d/o 70 solutions for the simulation *scenario 1* (as defined at the end of section 2.1.2), using the 3 above-introduced orbit scenarios. As the mean orbit altitudes of the considered orbit scenarios are not the same (cf. Tab. 1), we correct the solutions for the scenarios U3d5d_H and U5d_H by their difference in mean orbit altitude relative to the reference scenario 3d_H, in order to be able to extract the effect of the differing subcycle lengths on the retrieval errors. The height-corrected curves are shown as the dotted curves in Fig. 6.

Our altitude correction method is based on the assumption that the main observed quantity of the mission is the range rate, which is related to gravitational accelerations that decay as $\left(\frac{1}{r}\right)^{n+2}$ with increasing radius r (n is the SH degree). As the measured data is the sum of the $\left(\frac{1}{r}\right)^{n+2}$- dependent signal and the altitude-independent noise, the retrieval error (being the difference between the SH coefficients derived from the noisy data and the true SH coefficients of the signal) contains the radius-dependent factor r^{n+2}. In order to correct the altitude effect relative to the scenario 3d_H, we multiply the retrieval errors of the considered scenario by $\left(\frac{r_{\mathrm{ref}}}{r}\right)^{n+2}$, where r_{ref} and r are the mean radius of the polar and inclined pair of the reference scenario 3d_H and the scenario under consideration, respectively.

Comparing the dotted and solid curves of U3d5d_H and U5d_H in Fig. 6 shows that applying this height correction to the corresponding retrieval errors reduces the latter. The remaining error differences between the three scenarios can be explained by their differing ground track patterns: The ground track gaps of the polar pair in the scenario U3d5d_H lead to a slight degradation of the solution towards higher SH degrees, starting around $n = 25$. However, the coinciding ground track gaps of the polar and inclined pair in scenario U5d_H increase significantly the retrieval errors by almost one order of magnitude, starting at about $n = 10$.

Figure 7 shows that the 3-day retrieval errors are spatially correlated with the underlying double-pair ground track pattern of the respective scenario. Especially for scenario U5d_H, large retrieval errors occur in the regions of missing data centered at the equator. In general, we observe that gaps in the 3-day ground track especially impact the retrieval performance at low latitudes, while over

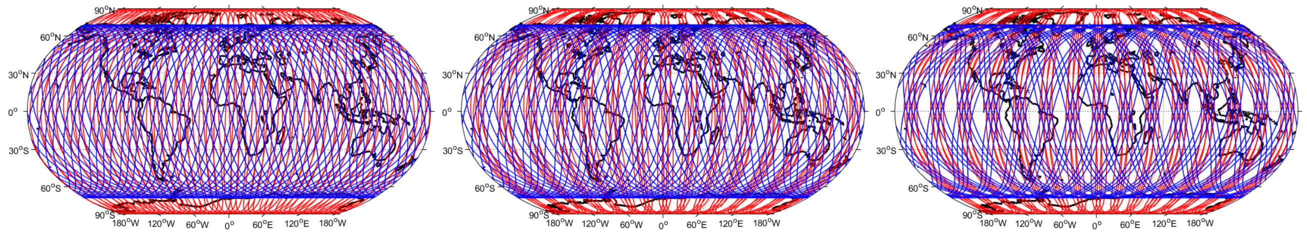

Figure 5. 3-day ground tracks of the polar (red) and inclined (blue) satellites corresponding to the orbit scenarios 3d_H (3-day subcycles, high altitude; left panel), U3d5d_H (uncoordinated 3-/5-day subcycles, high altitude; middle panel) and U5d_H (uncoordinated 5-day subcycles; right panel) (cf. Tab. 1).

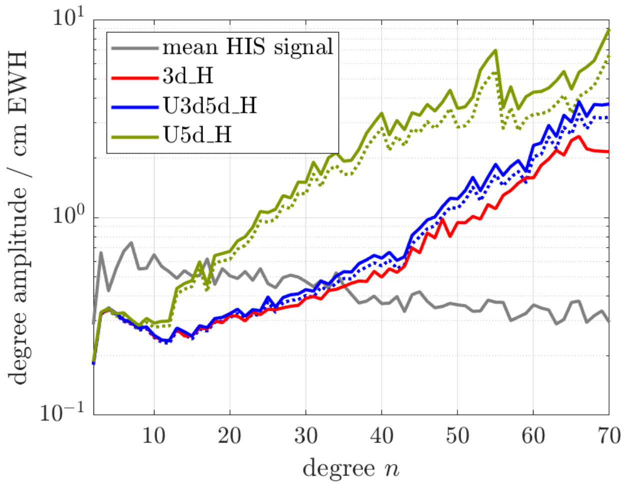

Figure 6. Degree error amplitudes of 3-day full signal and noise simulations for the Bender-type *scenario 1*, combining a polar in-line pair with GRACE-type noise and an inclined in-line pair with NGGM-type noise (cf. Eqs. (1) and (2)) based on 3d_H, U3d5d_H and U5d_H orbits as defined in Tab. 1. The corresponding 3-day orbit groundtracks are displayed in Fig. 5. The solid lines show the un-corrected curves, while the dotted lines represent the results after applying a factor correcting for the difference in mean orbit altitude relative to the reference scenario 3d_H (see text).

the poles, due to the ground track convergence, the retrieval errors of the three scenarios are comparable (not shown here).

After having demonstrated the importance of 3-day orbit subcycles for 3-day gravity retrieval, in the following we investigate if, in the case of both pairs having a 3-day subcycle, a common longitudinal drift rate between the two pairs is necessary in order to obtain subsequent 3-day solutions of homogeneous quality. To this end, we compare solutions based on our reference orbit scenario 3d_H (cf. panel a in Fig. 5 and the red curve in Fig. 6) to solutions based on U3d_H orbits. As specified by Tab. 1, the 3d_H orbits are constructed to have a common westward drift of the polar and inclined pair's orbits of about 3° per 3 days, such that the 3-day double-pair ground track forms a stable pattern that constantly moves westwards. For the U3d_H case, both pairs have 3-day subcycles but their orbits drift at different rates such that the double-pair ground track pattern is slightly different in each of the subsequent 3-day periods.

The top panel of Fig. 8 shows the results in terms of degree error amplitudes. The relative performance between the two scenarios is mainly determined by the differing inclination of the second satellite pair and is not analysed further at this point. For our purpose of analysing the impact of the coordination of the longitudinal drift between the two pairs on the relative quality of subsequent 3-day solutions, we concentrate on the error spread of the five respective individual solutions. To better visualise this error spread, we plot the relative deviation of the individual solutions from their mean in the bottom panel of Fig. 8. As shown by the thick lines in this panel, the retrieval errors of the individual 3-day solutions scatter by the same amount in the two scenarios. From this, we conclude that if stable subcycles matching the retrieval period are provided for both pairs, a common longitudinal drift between the ground tracks of the two pairs is not necessary to provide a homogeneous quality of subsequent 3-day solutions. That means, the double-pair ground track pattern does not need to be exactly equal among the subsequent 3-day solutions, as long as there is no strong spatial variation in the ground track density, as has been shown in the above-described analysis of the necessity of the orbit subcycles.

3.2.3 *Relative performance of the polar and inclined pair*

As stated in the introduction, the improved temporal resolution of gravity data from a double-pair mission will enable new applications requiring short-term gravity fields of a few days, as well as the application of processing methods such as the scheme proposed by (Wiese et al. 2011), in which low-SH degree daily gravity fields are co-estimated, thereby reducing temporal aliasing errors in the multi-day (e.g. monthly or weekly) solution. As described in section 2.1, this processing scheme allows to retrieve the full AO-HIS signal, avoiding the necessity of a background model-based de-aliasing. While there is ongoing research conducted on alternative approaches to the (Wiese et al. 2011) method, such as presented by (Abrykosov et al. 2022), the following investigation aims at demonstrating the performance of the established (Wiese et al. 2011) method for several possible MAGIC mission scenarios.

To this end, we investigate d/o 120 7-day solutions using the nominal and Wiese processing scheme (cf. section 2.1.1), where in the latter we use a maximum SH d/o of 15 for the daily Wiese solutions (DWS). The presented results are independent of the exact retrieval period chosen and were confirmed by corresponding monthly solutions (not included here). The maximum d/o of the DWS was chosen as optimum value in terms of the performance of the DWS and the multi-day solution.

Four scenarios differing by their accelerometer noise assumptions as well as their underlying orbits are defined: *scenario 1* is combined with 3d_H and 5d_LH orbits, while *scenario 2* is combined with 3d_H and 5d_LL orbits (for a definition of the two noise scenarios and details of the orbit scenarios, see the end of section 2.1.2 and Tab. 1, respectively). The differences in accelerometer noise levels and orbit heights of the satellites lead to varying relative weights of the two pairs' data in the double-pair NEQ systems.

As shown by Fig. 9, the 7-day solutions computed using the Wiese processing scheme reveal a specific error pattern that is not

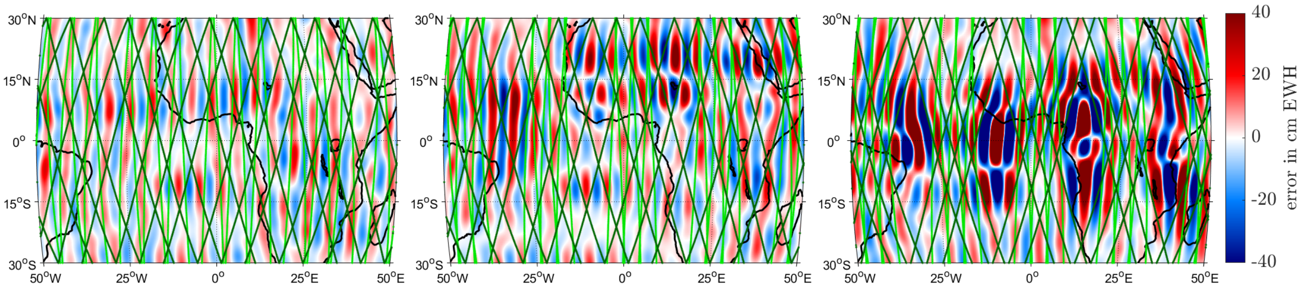

Figure 7. Retrieval errors of 3-day full signal and noise simulations for the same scenarios as in Fig. 6. The corresponding 3-day ground tracks of the polar and inclined satellite pair are displayed by the light and dark green lines, respectively. For the simulations using the U3d5d_H (middle panel) and U5d_H (right panel) orbits, the retrieval errors have been corrected for their difference in mean orbit altitude relative to the reference scenario 3d_H (left panel; for an explanation of the altitude correction, see text). All panels show the same grid section close to the equator and use the same colorbar.

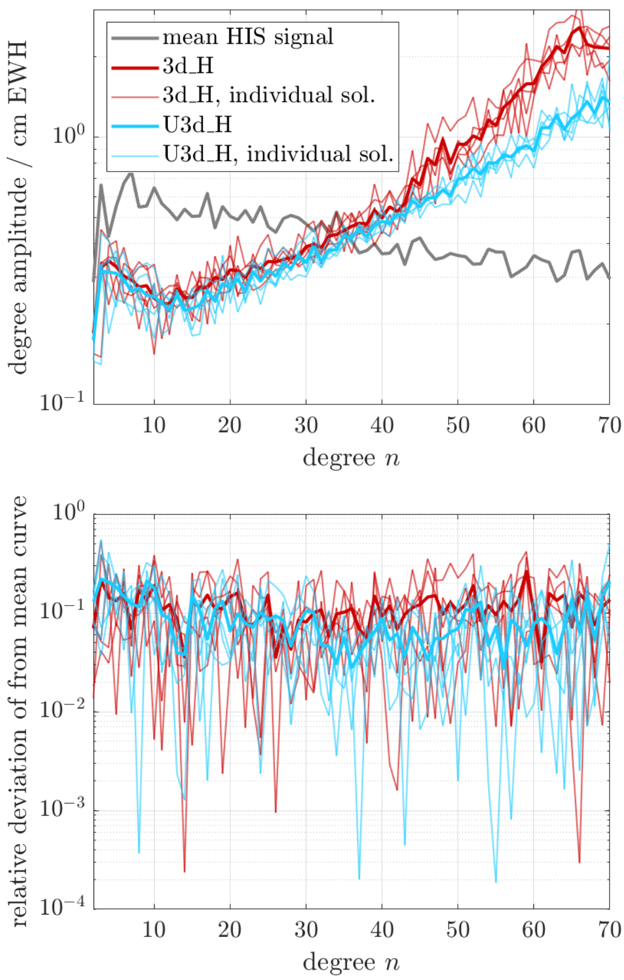

Figure 8. Top: The thin curves show the degree error amplitudes of five subsequent 3-day full signal and noise simulations for the Bender-type *scenario 1* combining a polar in-line pair with GRACE-type noise and an inclined in-line pair with NGGM-type noise (cf. Eqs. (1) and (2)) based on 3d_H and U3d_H orbits as defined in Tab. 1. The thick curves show the respective mean of the individual curves. Bottom: Deviation of the individual degree error amplitude curves shown in the top panel from their mean curve, divided by the mean curve. Also in the bottom panel, the thick curves show the mean of the individual curves.

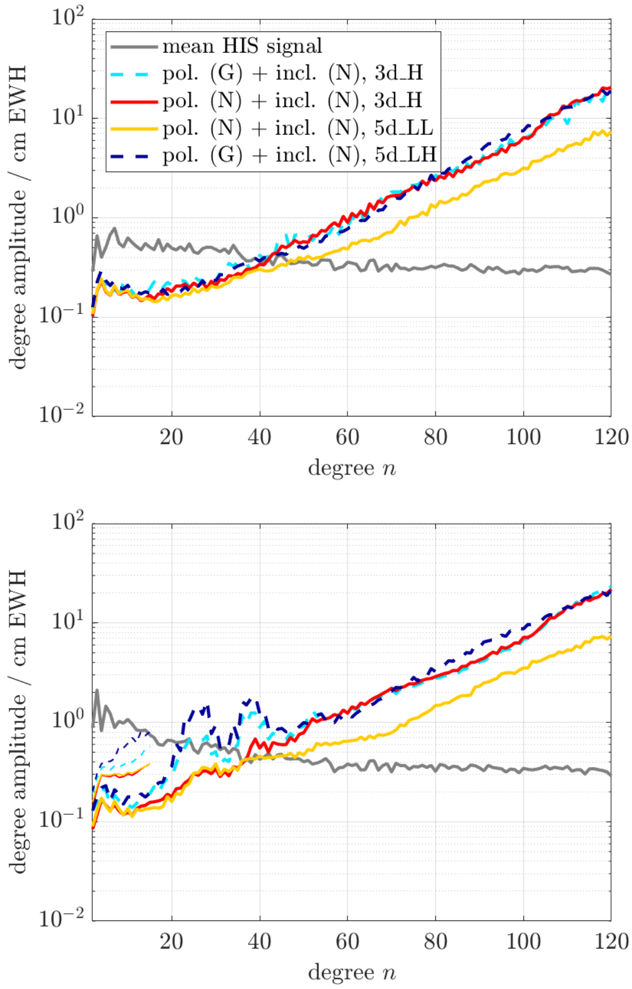

Figure 9. Degree error amplitudes of 7-day full signal and noise simulations for Bender-type scenarios combining a polar (pol.) and inclined (incl.) in-line pair, based on 3d_H, 5d_LL and 5d_LH orbits as defined in Tab. 1. G and N stand for GRACE- and NGGM-type noise assumptions as defined in Eqs. (1) and (2), respectively. Top: nominal processing results. Bottom: Wiese processing results, including the errors of the co-estimated d/o 15 daily Wiese solutions (DWS) as thin curves of the same color and line style as their corresponding d/o 120 7-day curves.

present in the nominal processing results. This error pattern consists of significantly larger errors around SH degrees 26 and 39, can be found in all four scenarios and turn out to be larger in amplitude the larger the relative contribution of the inclined pair's data to the double-pair solutions is. For example, the phenomenon is most severe for *scenario 1* using 5d_LH orbits, in which the data of the polar pair is given a particularly small weight compared to the inclined pair's data, both because of the polar satellites' larger accelerometer noise and their higher orbit altitude. Additionally, the retrieval errors of the DWS seem to be positively correlated with the amplitude of the described error pattern in the 7-day solutions. While the observed error pattern is clearly visible in the SH domain, it is not caused by increased errors in specific regions when considering spatial error grids (not shown here).

A thorough analysis on the causes of the error pattern is given in section 6.2 in the appendix. Essentially, the phenomenon is related to specific groups of sectorial coefficients of the multi-day solution being correlated to the coefficients of the co-estimated DWS. These large correlations originate from the NEQ system of the inclined pair in the Wiese processing scheme and degrade the double-pair solution if the weight of the inclined relative to the polar pair's NEQ system is (too) high.

To mitigate this problem, alternative methods to the processing scheme proposed by (Wiese et al. 2011) for the co-estimation of daily fields, such as the the DMD approach ((Abrykosov et al. 2022)) are currently investigated and assessed.

4 DISCUSSION

In this section, we briefly relate our above-presented findings to existing studies.

Following the comparison of various in-line and pendulum single- and double-pair configurations in section 3.1, we stated that a double in-line pair mission is the best choice for a next-generation gravity mission regarding performance and technical feasibility. This finding is consistent with (Elsaka et al. 2014), where besides the single- and double in-line pair and single-pendulum pair, additionally a cartwheel and a helix formation are analysed, and the best performance among the studied configurations is found for the double in-line pair.

After comparing 65° and 70° as inclination values for the second pair in a double-pair configuration in section 3.2.1, we found a trade-off between a reduction of striping noise at low latitudes and larger areas of increased retrieval errors centered around the poles if lowering the inclination value. As commented in section 3.2.1, optimising the inclination value of the second pair requires a performance metric taking into account the latitude-dependent accuracy requirements of various user groups. For example, in (Wiese et al. 2012), an optimum inclination value of 72° is determined based on the equally weighted global retrieval accuracy of hydrological, ice, and ocean bottom pressure signals. In addition to these scientific arguments, also the technical feasibility of launching the satellites into a certain orbit needs to be taken into account.

In section 3.2.2, we found that in order to enable short-term gravity solutions of a few days with homogeneous accuracy, an orbit control of the inclined pair is essential for MAGIC constellation short-term products of homogeneous quality. The fact that an uneven ground track density over the chosen retrieval period leads to a degradation of the retrieved gravity solution is known from GRACE real data processing: As the GRACE satellites were left free-drifting (besides an attitude control system maintaining the alignment of the two satellites), several of the derived monthly fields show a degraded performance, due to an unfavorable ground track ("deep resonance") within the respective months (e.g. (Wagner et al. 2006)).

As described in section 3.2.3, a co-estimation of low-degree daily gravity fields according to (Wiese et al. 2011) leads to increased retrieval errors in the case of double-pair solutions that are dominated by the data of the inclined pair, e.g. due to the choice of the orbit heights and noise assumptions for the two satellite pairs. To inspect if the observed error structure can also be found in previous work, we compared our results to some degree error amplitude plots shown by (Wiese et al. 2011), (Daras and Pail 2017) and (Purkhauser et al. 2020). In fact, the double-pair simulations performed in these studies assume similar orbit heights, as well as equal accelerometer and ranging noise levels for the two satellite pairs. As a consequence, there is no severe dominance of the inclined pair's NEQ system in the resulting double-pair solutions, which is why the correlations introduced by the polar gaps of the inclined pair do not impact the solutions in the same way as in some of the scenarios presented in our paper.

5 CONCLUSIONS AND OUTLOOK

Using numerical closed-loop simulations, this paper investigates key mission design aspects concerning the MAGIC satellite gravity mission, which is planned as the first realisation of a double-pair mission succeeding the successful single-pair missions GRACE and GRACE-FO. The considerable scientific value that the expected double-pair data will have, is demonstrated in this paper by showing the much reduced retrieval errors of unfiltered solutions. Additionally, the smaller required filter strength in the post-processing, having the advantage of less dampening of signal components by the filtering, is presented in the appendix of this paper. The latter might be beneficial to extract detail signals in smaller-scale hydrological catchments and specific features in the ocean such as boundary currents which usually show a large signal gradient.

The choice of the second pair's inclination was shown to strongly impact the latitude-dependency of the accuracy of the derived fields and therefore assessed to be a question of the (latitude-dependent) accuracy requirements of the various user communities.

As the expected double-pair data are planned to provide significant inputs to operational service applications, the role of orbit design aspects such as the maintenance of stable subcycles matching the desired retrieval period becomes more important compared to a single-pair mission to compute short-term gravity solutions of a few days. Based on 3-day solutions, we found that ground track gaps of the polar pair can be largely compensated by a homogeneous ground track coverage of the inclined pair, however coinciding ground track gaps of the polar and inclined pair significantly degrade the retrieved solution. Therefore, orbit control of the inclined pair is essential for MAGIC constellation short-term products of homogeneous quality. A common drift rate of the two pairs has been shown not to be necessary for a constant performance of subsequent short-term solutions.

Regarding the relative performance of the two satellite pairs, increased errors of solutions computed by co-estimating daily gravity fields according to (Wiese et al. 2011) were found in the case of double-pair scenarios that are strongly dominated by the inclined pair's data. This leads to the recommendation of a mission design combining two satellite pairs of comparable performance. In order to avoid the found degradation from the processing side, we propose the alternative approach by (Abrykosov et al. 2022), which is, however, still subject of further research.

Defining the mission design of MAGIC towards its realisation in more detail will require additional (simulation) studies, especially in cooperation with industrial partners building the measuring instruments and the satellites, as well as with scientists using the gravity data for specific applications. This strategy enables to optimise the mission setup taking into account its technical feasibility as well as the accuracy requirements from scientific user communities.

ACKNOWLEDGMENTS

The work presented in this paper was performed in the framework of the project "NGGM/MAGIC - SCIENCE SUPPORT STUDY DURING PHASE A", ESA-ESTEC, Contract 4000134613/21/NL/FF/ab funded by the European Space Agency.

We thank Pieter Visser for providing the osculating Kepler elements for the orbits underlying our simulations. We thank Markus Hauk for testing some of our findings regarding the artefacts in the Wiese solutions with the complementary simulation software at GFZ. We thank Petro Abrykosov for his advice and test simulation runs regarding the Data-driven multi-step self-de-aliasing approach (DMD). We thank Frank Flechtner, Josefine Wilms, Christoph Dahle, Günther March and Luca Massotti for valuable discussions during the project study.

We are very grateful for the valuable comments of two anonymous reviewers to the first version of this manuscript.

Finally, we acknowledge the provision of supercomputing resources by the Leibniz Supercomputing Centre (LRZ; Address: Boltzmannstraße 1, 85748 Garching bei München, Germany).

DATA AVAILABILITY

The data supporting the findings of this study are available upon request to the corresponding author.

REFERENCES

Abrykosov, P., Murböck, M., Hauk, M., Pail, R. & Flechtner, F., 2022. Data-driven multi-step self-de-aliasing approach for GRACE and GRACE-FO data processing, *Geophys. J. Int.*, **232**(2), 1006-1030. doi: 10.1093/gji/ggac340.

Bender, P. L., Wiese, D. & Nerem, R. S., 2008. A possible dual-GRACE mission with 90 degree and 63 degree inclination orbits, *Proceedings of the 3rd International Symposium on Formation Flying, Missions and Technologies*, ESA/ESTEC, Noordwijk, 23–25 April 2008, 1–6.

Cazenave, A., Dominh, K., Guinehut, S., Berthier, E., Llovel, W., Ramillien, G., Ablain, M. & Larnicol, G., 2009. Sea level budget over 2003-2008: A reevaluation from GRACE space gravimetry, satellite altimetry and Argo, *Glob. Planet. Chang.*, **65**(1-2), 83–88, doi: 10.1016/j.gloplacha.2008.10.004.

Cesare, S., Dionisio, S., Saponara, M., Bravo-Berguño, D., Massotti, L., da Encarnação, J. T. & Christophe, B., 2022. Drag and Attitude Control for the Next Generation Gravity Mission, *Remote Sens.*, **14**(12), 2916. doi: 10.3390/rs14122916.

Chambers D. P., Wahr, J., Tamisiea, M. E. & Nerem, R. S., 2010. Ocean mass from GRACE and glacial isostatic adjustment, *J. Geophys. Res. (Solid Earth)*, **115**(B11). doi: 10.1029/2010JB007530

Chen, J. L., Wilson, C. R., & Tapley, B. D., 2010. The 2009 exceptional Amazon flood and interannual terrestrial water storage change observed by GRACE, *Water Resour. Res.*, **46**(12). doi: 10.1029/2010wr009383.

Daras, I., Pail, R., Murböck, M. & Yi, W., 2015. Gravity field processing with enhanced numerical precision for LL-SST missions, *J. Geod.*, **89**(2), 99–110. doi: 10.1007/s00190-014-0764-2.

Daras, I., 2016. Gravity Field Processing Towards Future LL-SST Satellite Missions, *Deutsche Geodätische Kommission der Bayerischen Akademie der Wissenschaften*, Reihe C, Dissertationen, Heft 770, pp. 23–39. ISBN: 978-3-7696-5182-9.

Daras, I. & Pail, R., 2017. Treatment of temporal aliasing effects in the context of next generation satellite gravimetry missions, *J. Geophys. Res. (Solid Earth)*, **122**(9), 7343–7362. doi: 10.1002/2017jb014250.

Dionisio, S., Anselmi, A., Bonino, L., Cesare, S., Massotti, L. & Silvestrin, P., 2018. The "Next Generation Gravity Mission": challenges and consolidation of the system concepts and technological innovations, *SpaceOps Conference*. doi: 10.2514/6.2018-2495.

Dobslaw, H., Bergmann-Wolf, I., Dill, R., Forootan, E., Klemann, V., Kusche, J. & Sasgen, I., 2015. The updated ESA Earth System Model for future gravity mission simulation studies, *J. Geod.*, **89**(5), 505–513. doi: 10.1007/s00190-014-0787-8.

Dobslaw, H., Bergmann-Wolf, I., Forootan, E., Dahle, C., Mayer-Gürr, T., Kusche, J. & Flechtner, F., 2016. Modeling of present-day atmosphere and ocean non-tidal de-aliasing errors for future gravity mission simulations, *J. Geod.*, **90**(5), 423–436. doi: 10.1007/s00190-015-0884-3.

Elsaka, B., Raimondo, J.-C., Brieden, Ph., Reubelt, T., Kusche, J., Flechtner, F., Iran Pour, S., Sneeuw, N. & Müller, J., 2014. Comparing Seven Candidate Mission Configurations for Temporal Gravity Retrieval through Full-Scale Numerical Simulation, *J. Geod.*, **88**(1), 31–43. doi: 10.1007/s00190-013-0665-9.

Espinoza, J. C., Ronchail, J., Frappart, F., Lavado, W., Santini, W. & Guyot, J.-L., 2013. The major floods in the Amazonas River and tributaries (Western Amazon basin) during the 1970 - 2012 period: A focus on the 2012 flood, *J. Hydrometeorol.*, **14**(3), 1000-1008. doi: 10.1175/JHM-D-12-0100.1.

Flechtner, F., Neumayer, K. H., Dahle, C., Dobslaw, H., Güntner, A., Raimondo, J. C. & Fagiolini, E., 2016. What can be expected from the GRACE-FO laser ranging interferometer for earth science applications? *Surv. Geophys.*, **37**(2), 453–470. doi: 10.1007/s10712-015-9338-y.

Flechtner, F., Webb, F. & Watkins, M., 2017. Current status of the GRACE follow-on mission, *Geophys. Res. Abstr.*, **19**, EGU 2017–4566, EGU General Assembly 2017.

Forootan, E., Didova, O., Schumacher, M., Kusche, J. & Elsaka, B., 2014. Comparisons of atmospheric mass variations derived from ECMWF reanalysis and operational fields over 2003–2011, *J. Geod.*, **88**(5), 503–514. doi: 10.1007/s00190-014-0696-x.

Frappart, F., Papa, F., Da Silva, J. S., Ramillien, G., Prigent, C., Seyler, F., & Calmant, S., 2012. Surface freshwater storage and dynamics in the Amazon basin during the 2005 exceptional drought, *Environ. Res. Lett.*, **7**(4), 044010. doi: 10.1088/1748-9326/7/4/044010.

Frommknecht, B., Oberndorfer, H., Flechtner, F. & Schmidt, R., 2003. Integrated sensor analysis for GRACE - Development and validation. *Adv. Geosci.*, **1**, 57-63. doi: 10.5194/adgeo-1-57-2003.

Gruber, T., Murböck, M. & the NGGM-D Team, 2014. e2.motion - Earth System Mass Transport Mission (Square) - Concept for a Next Generation Gravity Field Mission, C.H. Beck.

Güntner, A., 2008. Improvement of Global Hydrological Models Using GRACE Data. *Surveys in Geophysics*, **29**(4-5), 375-397. doi: 10.1007/s10712-008-9038-y.

Haagmans, R., Siemes, C., Massotti, L., Carraz, O. & Silvestrin, P., 2020a. ESA's Mass-change And Gravity International Constellation concepts, *Rendiconti Lincei. Scienze Fisiche e Naturali*, **31**(S1), 15-25. doi: 10.1007/s12210-020-00875-0

Han, S.-C., Riva, R., Sauber, J. & Okal, E., 2013. Source parameter inversion for recent great earthquakes from a decade-long observation of global gravity fields, *J. Geophys. Res.*, **118**(3), 1240–1267. doi: 10.1002/jgrb.50116.

Hauk, M. & Pail, R., 2019. Gravity field recovery using high-precision, high–low inter-satellite links, *Remote Sens.*, **11**(5), 537. doi: 10.3390/rs11050537.

Hauk, M. & Wiese, D. N., 2020. New Methods for Linking Science Objectives to Remote Sensing Observations: A Concept Study Using Single- and Dual-Pair Satellite Gravimetry Architectures, *Earth and Space Science*, **7**(3). doi: 10.1029/2019ea000922.

Horvath, A., Murböck, M., Pail, R. & Horwath, M., 2018. Decorrelation of GRACE time variable gravity field solutions using full covariance information, *Geosciences*, **8**(9), 323. doi: 10.3390/geosciences8090323.

Iran Pour, S., Reubelt, T., Sneeuw, N., Daras, I., Murböck, M., Gruber, T., Pail, R., Weigelt, M., van Dam, T., Visser, P., Encarnação, J.T., van den IJssel, J., Tonetti, S., Cornara, S. & Cesare, S., 2015. Assessment of satellite constellations for monitoring the variations in earth gravity field – SC4MGV, ESA – ESTEC Contract No. AO/1-7317/12/NL/AF, Final Report.

Ivins, E. R., James, T. S., Wahr, J., Schrama, E. J. O., Landerer, F. W. & Simon, K. M., 2013. Antarctic contribution to sea level rise observed by GRACE with improved GIA correction, *J. Geophys. Res. (Solid Earth)*, **118**(6), 3126-3141. doi: 10.1002/jgrb.50208.

Kornfeld, R. P., Arnold, B. W., Gross, M. A., Dahya, N. T. & Klipstein, W. M., 2019. GRACE-FO: the gravity recovery and climate experiment follow-on mission, *J. Spacecraft Rockets*, **56**(3), 931-951. doi: 10.2514/1.a34326.

Lenoir, B., Lévy, A., Foulon, B., Lamine, B., Christophe, B.& Reynaud, S., 2011. Electrostatic accelerometer with bias rejection for gravitation and Solar System physics, *Adv. SpaceRes.*, **48**(7), 1248–1257. doi: 10.1016/j.asr.2011.06.005.

Luthcke, S. B., Sabaka, T., Loomis, B., Arendt, A., McCarthy, J. & Camp, J., 2013. Antarctica, Greenland, and Gulf of Alaska land-ice evolution from an iterated GRACE global mascon solution, *J. Glaciol.*, **59**(216), 613–631. doi: 10.3189/2013jog12j147.

Lombard, A., Garcia, D., Ramillien, G., Cazenave, A., Biancale, R., Lemoine, J. M., Flechtner, F., Schmidt, R. & Ishii, M., 2007. Estimation of steric sea level variations from combined GRACE and Jason-1 data *Earth Planet. Sci. Lett.*, **254**(1-2), 194–202. doi: 10.1016/j.epsl.2006.11.035.

MAGIC MRD, 2020. *Mission Requirement Document (MRD) Next Generation Gravity Mission as a Mass change And Geosciences International Constellation (MAGIC)*, `https://esamultimedia.esa.int/docs/EarthObservation/MAGIC_NGGM_MCDO_MRD_v1_0-signed2.pdf`, Issue 1.0, 30 October 2020, ESA-EOPSM-FMCC-MRD-3785, 2020.

Massotti, L., Amata, G. B., Anselmi, A., Cesare, S., Martimort, P. & Silvestrin, P., 2020. Next Generation Gravity Mission: status of the design and discussion on alternative drag compensation scenarios, *Sensors, Systems, and Next-Generation Satellites XXIV, SPIE*. doi: 10.1117/12.2573924.

Massotti, L., Siemes, C., March, G., Haagmans, R. & Silvestrin, P., 2021. Next Generation Gravity Mission Elements of the Mass Change and Geoscience International Constellation: From Orbit Selection to Instrument and Mission Design, *Remote Sens.*, **13**(19), 3935. doi: 10.3390/rs13193935.

Mayer-Gürr, T., 2006. Gravitationsfeldbestimmung aus der Analyse kurzer Bahnbögen am Beispiel der Satellitenmissionen CHAMP und GRACE, url: http://hss.ulb.uni-bonn.de/2006/0904/0904.htm.

Mayer-Gürr, T., Pail, R., Gruber, T., Fecher, T., Rexer, M., Schuh, W.-D., Kusche, J., Brockmann, J.-M., Rieser, D., Zehentner, N., Kvas, A., Klinger, B., Baur, O., Höck, E., Krauss, S., Jäggi, A., 2015. The combined satellite gravity field model GOCO05s, *Geophys. Res. Abstracts*, **17**, EGU2015-12364, European Geosciences Union General Assembly 2015 (Vienna, Austria). doi: 10.13140/RG.2.1.4688.6807.

Metzler, B. & Pail, R., 2005. GOCE Data Processing: The Spherical Cap Regularization Approach, *Studia Geophysica et Geodaetica*, **49**(4), 441–462. doi: 10.1007/s11200-005-0021-5.

Pail, R. et al., 2015. Observing Mass Transport to Understand Global Change and to Benefit Society: Science and User Needs – An international multi-disciplinary initiative for IUGG, *Deutsche Geodätische Kommission der Bayerischen Akademie der Wissenschaften*, Heft 320, ISBN 978-3-7696-8599-2, München.

Pail, R., Bamber, J., Biancale, R., Bingham, R., Braitenberg, C., Eicker, A., Flechtner, F., Gruber, T., Güntner, A., Heinzel, G., Horwath, M., Longuevergne, L., Müller, J., Panet, I., Savenije, H., Seneviratne, S., Sneeuw, N., van Dam, T. & Wouters, B., 2019. Mass variation observing system by high low intersatellite links (MOBILE) – a new concept for sustained observation of mass transport from space, *J. Geod. Sci.*, **9**(1), 48-58. doi:10.1515/jogs-2019-0006.

Pail, R., Yeh, H.-C., Feng, W., Hauk, M., Purkhauser, A., Wang, C., Zhong, M., Shen, Y., Chen, Q., Luo, Z., Zhou, H., Liu, B., Zhao, Y., Zou, X., Xu, X., Zhong, B., Haagmans, R., Xu, H., 2019. Next-Generation Gravity Missions: Sino-European Numerical Simulation Comparison Exercise. *Remote Sens.* **11**(22), 2654. doi: 10.3390/rs11222654.

Panet, I., Pajot-Métivier, G., Greff-Lefftz, M., Métivier, L., Diament, M. & Mandea, M., 2014. Mapping the mass distribution of Earth's mantle using satellite-derived gravity gradients, *Nat. Geosci.*, **7**(2), 131–135. doi: 10.1038/ngeo2063.

Panet, I., Narteau, C., Lemoine, J.-M., Bonvalot, S., & Remy, D., 2022. Detecting preseismic signals in GRACE gravity solutions: Application to the 2011 Tohoku Mw 9.0 earthquake, *J. Geophys. Res. (Solid Earth)*, **127**(8). doi: 10.1029/2022jb024542.

Peltier W. R., 2009. Closure of the budget of global sea level rise over the GRACE era: the importance and magnitudes of the required corrections for global glacial isostatic adjustment, *Quat. Sci. Rev.*, **28**(17-18), 1658–1674. doi: 10.1016/j.quascirev.2009.04.004

Pfaffenzeller N., Pail R., 2023. Small satellite formations and constellations for observing sub-daily mass changes in the Earth system. *Geophys. J. Int.* **234**(3), 1550-1567. doi: 10.1093/gji/ggad132.

Purkhauser, A. F., Pail, R., 2019. Next generation gravity missions: near-real time gravity field retrieval strategy, *Geophys. J. Int.*, **217**(2) 1314–1333. doi: 10.1093/gji/ggz084.

Purkhauser, A. et al., 2019. Additional Constellation & Scientific Analysis of the Next Generation Gravity Mission Concept "ADDCON" Technical Note 2 (TN2) - 1 vs 2 pair simulations. ESA Contract AO/1-7317/12/NL/AF.

Purkhauser, A. F., Siemes, C. & Pail, R., 2020. Consistent quantification of the impact of key mission design parameters on the performance of next-generation gravity missions, *Geophys. J. Int.*, **221**(2), 1190-1210. doi: 10.1093/gji/ggaa070.

Ramillien, G., Lombard, A., Cazenave, A., Ivins, E. R., Llubes, M., Remy, F. & Biancale, R., 2006. Interannual variations of the mass balance of the Antarctica and Greenland ice sheets from GRACE. *Glob. Planet. Chang.*, **53**(3), 198-208. doi: 10.1016/j.gloplacha.2006.06.003.

Ray, R., 2008. GOT4.7. Extension of Ray R (1999) A global ocean tide model from Topex/Poseidon altimetry GOT99.2., *NASA Tech Memo 209478*.

Rodell, M., Famiglietti, J. S., Wiese, D. N., Reager, J. T., Beaudoing, H. K., Landerer, F. W. & Lo, M. H., 2018. Emerging trends in global freshwater availability, *Nature*, **557**(7707), 651–659. doi: 10.1038/s41586-018-0123-1.

Savcenko, R. & Bosch, W., 2012. EOT11a - empirical ocean tide model from multi-mission satellite altimetry, *DGFI-Report No.89*.

Schmidt, R., Flechtner, F., Meyer, U., Neumayer, K.-H., Dahle, Ch., König, R.& Kusche, J., 2008. Hydrological Signals Observed by the GRACE Satellites, *Surveys in Geophysics*, **29**(4-5), 319-334. doi: 10.1007/s10712-008-9033-3.

Schrama, E. J. O., Wouters, B. & Lavallée, D. A., 2007. Signal and noise in Gravity Recovery and Climate Experiment (GRACE) observed surface mass variation, *J. Geophys. Res.*, **112**(B8). doi: 10.1029/2006jb004882.

Shampine, L. F. & Gordon, M. K., 1975. Computer Solution of Ordinary Differential Equations: The Initial Value Problem. San Francisco: W.H. Freeman.

Sharifi, M., Sneeuw, N. & Keller, W., 2007. Gravity recovery capability of four generic satellite formations, *Gravity Field of the Earth. General Command of Mapping*, S18, 211-216, eds.: A. Kilicoglu and R. Forsberg.

Sneeuw, N. & van Gelderen, M., 1997. The polar gap. In: Sansó, F., Rummel, R. (eds) Geodetic Boundary Value Problems in View of the One Centimeter Geoid. Lecture Notes in Earth Sciences, vol 65. Springer, Berlin, Heidelberg. doi: 10.1007/BFb0011717.

Sneeuw, N., Sharifi, M. A. & Keller, W., 2008. Gravity recovery from formation flight missions. In: Xu, P., Liu, J., Dermanis, A. (eds) VI Hotine-Marussi Symposium on Theoretical and Computational Geodesy. International Association of Geodesy Symposia, vol 132. Springer, Berlin, Heidelberg. doi: 10.1007/978-3-540-74584-6_5.

Srinivasan, M., Rodell, M., Reager, J. T., Rogers, L., Doorn, B., 2019. Mass Change Mission Applications - Assessing User Needs for the Next NASA Mass Change Designated Observable (MCDO) Mission, American Geophysical Union (AGU) Fall Meeting, San Francisco.

Tapley, B. D., Bettadpur, S., Watkins, M. & Reigber, C., 2004. The gravity recovery and climate experiment experiment: mission overview and early results, *Geophys. Res. Lett.*, **31**(9). doi: 10.1029/2004gl019920.

Taylor, R. G., Scanlon, B., Döll, P., Rodell, M., Van Beek, R., Wada, Y., Longuevergne, L., Leblanc, M., Famiglietti, J. S., Edmunds, M., Konikow, L., Green, T. R., Chen, J., Taniguchi, M., Bierkens, M. F. P., MacDonald, A., Fan, Y., Maxwell, Reed M. / Yechieli, Y., Gurdak, J. J., Allen, D. M., Shamsudduha, M., Hiscock, K., Yeh, P. J.-F., Holman, I. & Treidel, H., 2013. Ground water and climate change *Nat. Clim. Chang.*, **3**(4), 322-329. doi: 10.1038/nclimate1744.

TUM IAPG, 2020. Simulation studies for a Mass change And Geosciences International Constellation (MAGIC). url: https://www.asg.ed.tum.de/iapg/magic/

Velicogna, I., Sutterley, T. C. & van den Broeke, M. R., 2014. Regional acceleration in ice mass loss from Greenland and Antarctica using GRACE time-variable gravity data, *Geophys. Res. Lett.*, **41**(22), 8130–8137. doi: 10.1002/2014gl061052.

Visser, P., Sneeuw, N., Reubelt, T., Losch, M. & van Dam, T., 2010. Spaceborne gravimetric satellite constellations and ocean tides: aliasing effects, *Geophys. J. Int.*, **181**(2), 789–805. doi: 10.1111/j.1365-246x.2010.04557.x.

Wagner, C., McAdoo, D., Klokočnìk, J. & Kostelecký, J., 2006. Degradation of Geopotential Recovery from Short Repeat-Cycle Orbits: Application to GRACE Monthly Fields, *J. Geod.*, **80**(2), 94-103. doi: 10.1007/s00190-006-0036-x.

Wahr, J., Moleneer, M. & Bryan, F., 1998. Time variability of the Earth's gravity field: hydrological and oceanic effets and their possible detection using GRACE, *J. Geophys. Res. (Solid Earth)*, **103**(B12). 30205-30229, doi:10.1029/98jb02844.

Wiese, D. N., Folkner, W. M. & Nerem, R. S., 2009. Alternative mission architectures for a gravity recovery satellite mission, *J. Geod.*, **83**(6), 569–581. doi: 10.1007/s00190-008-0274-1.

Wiese D. N., Visser P. & Nerem R. S., 2011. Estimating low resolution gravity fields at short time intervals to reduce temporal aliasing errors. *Adv. Space Res.*, **48**(6), 1094–1107. doi: 10.1016/j.asr.2011.05.027.

Wiese, D. N., Nerem, R. & Han, S.-C., 2011a. Expected improvements in determining continental hydrology, ice mass variations, ocean bottom pressure signals, and earthquakes using two pairs of dedicated satellites for temporal gravity recovery, *J. Geophys. Res. (Solid Earth)*, **116**(B11). doi: 10.1029/2011jb008375.

Wiese, D. N., Nerem, R. & Lemoine, F., 2012. Design considerations for a dedicated gravity recovery satellite mission consisting of two pairs of satellites, *J. Geod.*, **86**(2), 81–98. doi: 10.1007/s00190-011-0493-8.

Wiese, D. N. & Hauk, M., 2019. New methods for linking science objectives to mission architectures: A case study comparing single and dual-pair satellite gravimetry mission architectures, G51B-0577, American Geophysical Union (AGU) Fall Meeting, San Francisco.

Wiese, D. N., Bienstock, B., Blackwood, C., Chrone, J., Loomis, B. D., Sauber, J., Rodell, M., Baize, R., Bearden, D., Case, K., Horner, S., Luthcke, S., Reager, J. T., Srinivasan, M., Tsaoussi, L., Webb, F., Whitehurst, A. & Zlotnicki, V., 2022. The mass change designated observable study: Overview and results. *Earth and Space Science*, **9**(8). doi: 10.1029/2022ea002311.

Wouters, B., Gardner, A. S. & Moholdt, G., 2019. Global Glacier Mass Loss During the GRACE Satellite Mission (2002-2016). *Frontiers in Earth Science*, **7**. doi: 10.3389/feart.2019.00096.

6 APPENDIX

6.1 Impact of post-processing on single- and double-pair solutions

In addition to our considerations of unfiltered solutions for various single- and double-pair scenarios in section 3.1, this section demonstrates the benefit of double-pair data compared to single-pair data of GRACE(-FO) type based on post-processed solutions. To this end, VADER filters are constructed and applied to d/o 120 7-day gravity fields retrieved from a single- and a double-pair scenario, both being based on 3d_H orbits. Specifically, we are interested in the magnitude of the error components of the filtered solutions as introduced in section 2.2, Eq. (6). As single-pair scenario, a polar pair with GRACE-type accelerometer noise as defined by Eq. (1) is considered. As double-pair scenario, the combination of a polar and an inclined pair, both with NGGM-type accelerometer noise assumptions as defined by Eq. (2), is considered.

The results for the single- (double-) pair scenario are plotted in the left (right) panel of Fig. 10. By comparing the error levels between the two scenarios before (blue solid curves) and after the filtering (blue dotted curves), it becomes visible that the post-processing significantly reduces the performance difference between the single- and the double-pair scenario. This shows that the filter constructed based on the single-pair NEQs is much stronger than the double-pair filter. This difference in filter strength between the two scenarios is caused by the different error levels of the unfiltered solutions, considered in the filter design by the matrix N (cf. Eq. 5).

Considering the error components of the VADER-filtered double-pair solution in Fig. 10 (right panel) reveals that up to about $n = 60$, the error Δx_α (blue dotted curve) mainly consists of the contribution of the (filtered) solution error $W_\alpha \Delta x$ (green curve). For larger degrees, the signal dampening component $(W_\alpha - 1)x_{\text{HIS}}$ (black curve) starts to dominate the error of the filtered double-pair solution Δx_α.

In contrast, in the case of the single-pair scenario (left panel of Fig. 10), as the VADER filter is stronger here, the error of the VADER-filtered solution Δx_α (blue dotted curve) is mainly determined by the signal dampening effect (black curve) over the complete SH spectrum. This means that by applying an optimised VADER filter to single-pair solutions leads to a significant loss of signal components in them. As can be seen by comparing the results for the two scenarios, this effect can be significantly mitigated by double-pair constellations such as MAGIC, where much less post-processing is required to reduce the errors in the solution, thereby also leading to a smaller signal dampening effect.

The much weaker signal dampening in the post-processing of double-pair solutions can be considered as a significant advantage in view of scientific user applications, as the filtered double-pair solutions contain a better-resolved signal compared to single-pair solutions. This of course holds under the assumption that the signal components remaining in the filtered solutions can be in some way distinguished from the remaining error components.

These results demonstrate that although the error levels of the filtered single- and double-pair solution are very similar, data from a double-pair mission such as the planned MAGIC mission require weaker filters, i.e. much less post-processing, thereby causing a much smaller effect of signal dampening due to the filtering.

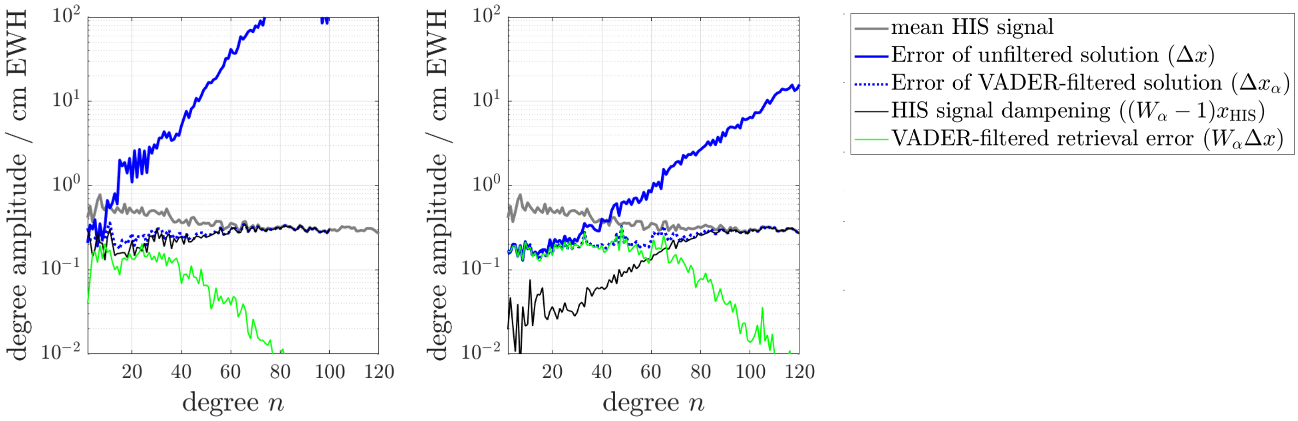

Figure 10. Degree error amplitudes of 7-day full signal and noise simulations for two scenarios based on 3d_H orbits. The left panel shows the results obtained for a single polar pair with a GRACE-type accelerometer. The right panel shows the results for the Bender-type *scenario 2* combining a polar and an inclined pair both with NGGM-type accelerometers. In both panels, the black and the green thin curves visualise the error components of the respective VADER-filtered solution (cf. Eq. 6), i.e. the sum of the black and the green curve equals the dotted blue curve in each of the panels.

6.2 Origin of the error pattern when co-estimating daily gravity fields

As observed in section 3.2.3, double-pair solutions dominated by the inclined pair's data reveal a specific error pattern when co-estimating daily gravity solutions according to (Wiese et al. 2011). As revealed by Fig. 9, the observed error pattern limits the spatial resolution of the 7-day Wiese solutions compared to the nominal results. Therefore, this section gives a detailed analysis and interpretation on the cause of the phenomenon, considering d/o 100 7-day solutions for *scenario 1* using 5d_LH orbits, as this scenario showed the largest degradation in Fig. 9 (bottom).

The top and bottom left panels of Fig. 11 show the retrieval errors of corresponding nominal and Wiese solutions in the SH domain, respectively. It can be seen that the groups of coefficients causing the error pattern observed in Fig. 9 (bottom) are (near-) sectorial. Our analysis in section 3.2.3 suggested a relationship between the occurrence of the error pattern and an increased relative weight of the inclined pair's data in the double-pair NEQ system. Therefore, we additionally compute corresponding double-pair solutions in the case of a 10^{14}-fold increased relative weight of the inclined pair's NEQ system, in order to test if in this case the error pattern becomes provoked even more. The results are shown by the right panels of Fig. 11. Indeed, the Wiese solution (bottom right panel) shows amplified retrieval errors of the groups of (near-) sectorial coefficients building the error pattern in the original double-pair Wiese solution (bottom left panel). In contrast, this error pattern is not present in the corresponding nominal solution (top right panel). This suggests that increasing the weight of the inclined pair's data in a double-pair NEQ system can lead to a degradation of retrieved gravity fields in the case that daily solutions are co-estimated.

As nominal solutions are not affected by the phenomenon, the latter seems to be related to the parameter co-estimation procedure in the Wiese processing. To investigate that further, we have a closer look at the Wiese solution corresponding to the bottom left panel of Fig. 11 in the following. The blue curve in Fig. 13 shows the degree error amplitudes for this scenario clearly showing the investigated error pattern. Figure 12 (a) visualises the correlations of the SH coefficients of that solution. The shown correlation matrix Corr is computed based on the full (i.e., including both the DWS and weekly solution coefficients) Wiese NEQ matrix $A^T PA$ of the double-pair solution as follows:

$$\begin{aligned} \mathrm{Cof} &= \left(A^T PA\right)^{-1} \\ \mathrm{Corr}_{ij} &= \frac{\mathrm{Cof}_{ij}}{\sqrt{\mathrm{Cof}_{ii}\cdot \mathrm{Cof}_{jj}}}\,. \end{aligned} \tag{7}$$

The exact coefficient ordering in the matrices shown by Fig. 12 is explained in detail in the corresponding figure caption. Most importantly, we marked the beginning of the coefficient blocks of the seven DWS and the 7-day solution by a “0”. Also, to be able to detect the sectorial coefficients of the 7-day solution, even-order sectorial coefficients were marked by ticks. Indeed, Fig. 12 (a, see the blue-boxed matrix part) shows increased correlations between the coefficients of the DWS and the groups of sectorial coefficients of the 7-day solution that show larger retrieval errors in Fig. 11 (bottom left) and Fig. 13 (blue curve).

The causal relationship between the above-described correlations and the error structure in the weekly Wiese solution is demonstrated in the following by considering two additional cases:

(1) a double-pair solution involving a 100-fold increased relative weight of the polar pair's NEQ system, visualised by Fig. 12 (b) and the red curves in Fig. 13, and

(2) a double-pair solution in which the off-diagonal NEQ entries representing correlations between the coefficients of the DWS and the 7-day solution are set to zero before the inversion, visualised by Fig. 12 (c) and the orange curves in Fig. 13.

Two facts are demonstrated by these two additional tests:

Firstly, the fact that the prominent correlation structure between DWS and multi-day solution can be attenuated by increasing the relative weight of the polar pair's NEQ system (against its “inherent” weight determined by the orbit height and noise assumptions for the polar satellites). This can be observed by comparing the first two panels of Fig. 12: the considered correlations in the blue-boxed matrix parts are significantly damped in the middle compared to the top panel.

Secondly, the fact that there is a direct causal relationship between these correlations and the specific error structure degrading

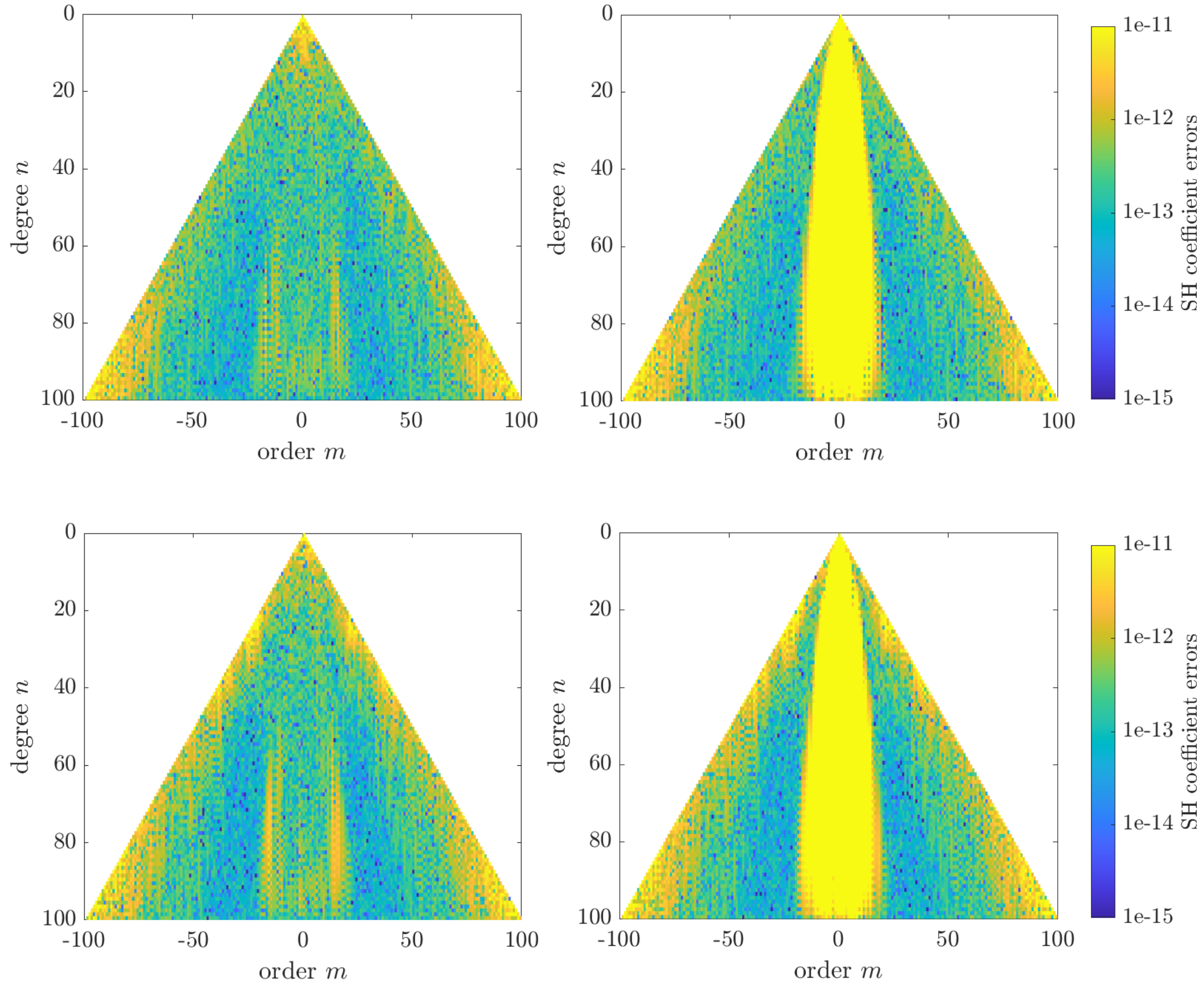

Figure 11. Retrieval errors of 7-day full signal and noise simulations for the Bender-type *scenario 1*, combining a polar pair with GRACE-type accelerometer noise and an inclined pair with NGGM-type accelerometer noise (cf. Eqs. (1) and (2)), using 5d_LH orbits (cf. Tab. 1). The top (bottom) panels display solutions obtained using the nominal (Wiese) processing scheme, respectively. The left panels show the solutions in the standard double-pair case, where the polar and inclined pair's NEQ systems are equally weighted. The right panels show the double-pair solutions using a ratio of the weights of the polar by the inclined pair's NEQs of 10^{-14}, to provide a measure for the performance of the respective single-inclined pair solutions. The colorbar is the same for all panels.

the Wiese solutions. This is visualised by comparing the blue to the red and orange curves in Fig. 13: If the correlations in the double-pair system are reduced or set to zero (cf. Fig. 12 (b) and (c)), the retrieval errors both of the degraded 7-day coefficients and of the DWS coefficients decrease (cf. red and orange curves in Fig. 13).

Interestingly, we note that a relative up-weighting of the polar pair's NEQ system by a factor of 100 even provides an overall improvement of the double-pair solution, as shown by the red curves in Fig. 13 (increasing the up-weighting factor even more however leads to an increase of retrieval errors over the complete SH spectrum, which is not shown here). As to be expected, setting the correlations to zero before the inversion globally destroys the solution, as shown by the orange lines in Fig. 13.

Summarising the above findings, the found phenomenon of increased retrieval errors when co-estimating daily solutions seems to be caused by correlations between the coefficients of the DWS and the multi-day solution, which originate from the NEQ system of the inclined pair in the Wiese processing scheme. As known from (Sneeuw and van Gelderen 1997) and (Metzler and Pail 2005), gravity solutions derived from data that are measured by an inclined orbiting satellite and therefore include data gaps over the poles, show larger errors for a group of near-zonal SH coefficients forming a triangular shape in the SH domain. These larger errors of near-zonal coefficients are caused by correlations between low and high-degree SH base functions in the data-covered area that affect the retrieval performance of increasing orders for increasing degrees. This phenomenon is attenuated when decreasing the maximum estimated SH degree (as this reduces the number of SH base functions that could be correlated).

In the present case, as the d/o 15 DWS are co-estimated along with the d/o 100 7-day solution, the maximum SH degree of the overall NEQ system that determines the polar gap-related correlations and error amplitudes of the near-zonal coefficients (also in the DWS) is $N_{\max} = 100$. This is visualised by Fig. 14 (left) where

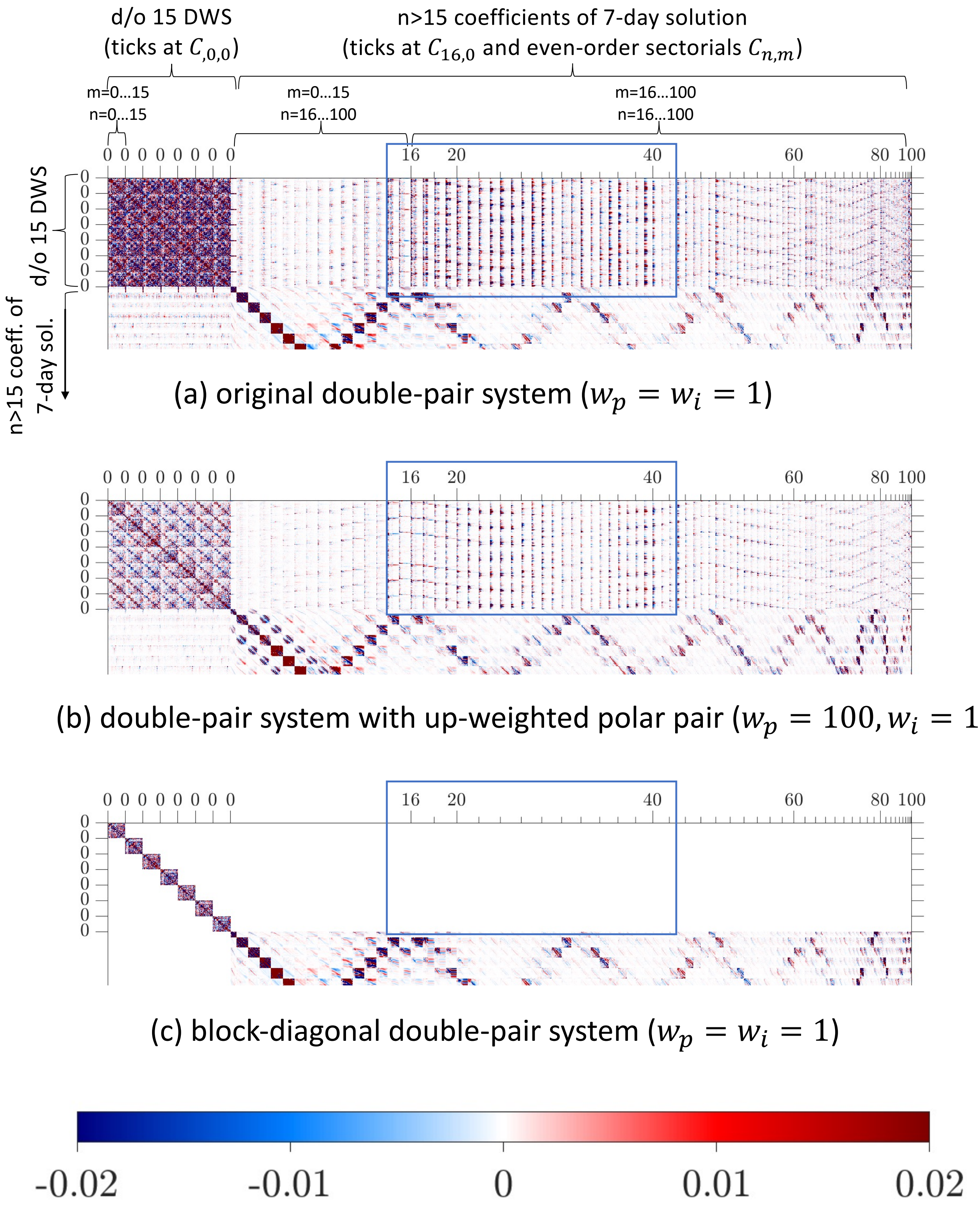

Figure 12. Each of the three panels shows the topmost part (cut after several rows) of a correlation (i.e. quadratic) matrix computed for a specific Wiese processing case. In all cases, a d/o 100 (d/o$_{\mathrm{DWS}}$ = 15) 7-day full signal and noise simulation was performed for the Bender-type *scenario 1*, combining a polar in-line pair with GRACE-type noise and an inclined in-line pair with NGGM-type noise (cf. Eqs. (1) and (2)), based on 5d_LH orbits (cf. Tab. 1).

(continues on next page)

Figure 12. (continued from previous page)
Starting from the top left in each of the matrices, the first block (composed of 7 sub-blocks) of rows/columns corresponds to the degree 0 to 15 SH coefficients of the seven co-estimated daily fields. The start of these d/o 15 coefficient sets it indicated by the first seven "0" ticks, each marking the respective $C_{0,0}$ coefficient. The remaining rows/columns (starting with the eighth "0" tick marking the $C_{16,0}$ coefficient of the d/o 100 7-day solution) correspond to the degree 16 to 100 coefficients of the 7-day solution. The coefficients within each of the 7 + 1 blocks are ordered by ascending SH order, then by ascending SH degree and afterwards, firstly $C_{n,m}$ and secondly $S_{n,m}$ coefficients are taken. Ticks are only provided for the $C_{0,0}$ coefficients of the DWS, the $C_{16,0}$ coefficient of the 7-day solution, as well as for sectorial ($n = m$) coefficients of even orders between 16 and 100. All tick labels represent the SH order m of the respective coefficient.
The top panel shows the matrix part for the original double-pair system ($w_p = w_i = 1$), the middle panel for the double-pair system using a 100-fold up-weighting of the polar pair's NEQ system relative to the inclined pair's NEQ system ($w_p = 100$, $w_i = 1$) and the bottom panel for the double-pair system where the correlations between the DWS coefficients and the higher-degree coefficients of the 7-day solution have been set to zero in the NEQ matrix to obtain a block-diagonal NEQ system, respectively. w_p and w_i represent the relative weights of the NEQ systems of the polar and inclined pair, respectively. All panels use the same colourbar.

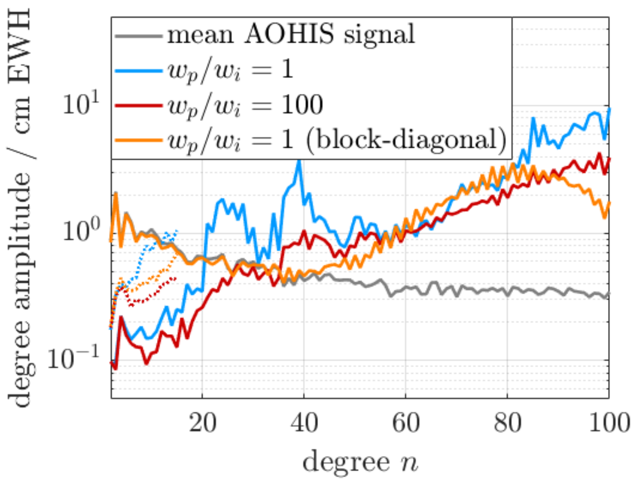

Figure 13. The blue, red and orange curves show the degree error amplitudes of the solutions associated with the correlation matrices shown in panels a, b and c of Fig. 12, respectively. For a description of the simulation details, see the caption of Fig. 12. Solid (dotted) curves show the errors of the 7-day solutions (DWS), respectively.

the retrieval errors of the first d/o 15 DWS estimated along the 7-day solution given by Fig. 11 (bottom right) are plotted. As for this inversion, the relative weight of the inclined pair's NEQ system has been increased to 10^{14}, the solution can be regarded as showing the retrieval performance of the inclined pair's data alone. For comparison, Fig. 14 (right) shows the retrieval errors of a d/o 15 stand-alone daily solution solely based on data of the inclined pair. It can clearly be seen that the single-inclined pair DWS is strongly affected by the data gaps over the poles, due to correlations of the $n < 16$ coefficients of the DWS and the $n = 16 - 100$ remaining coefficients. If no higher-degree coefficients are co-estimated, the maximum SH degree of the NEQ system, determining the amplitude of the near-zonal coefficient errors is $N_{\text{max}} = 15$ and the polar gap does not degrade the coefficients of the daily solution.

This observation completes our understanding of the investigated increased errors in solutions computed using the Wiese processing scheme: In double-pair systems that are strongly dominated by the data of the inclined pair, correlations between the SH coefficients of the co-estimated daily and multi-day solutions which originate in the polar gaps of the inclined pair lead to a degradation of the DWS as well as larger errors for specific groups of near-sectorial coefficients of the multi-day solution.

In order to find an improved processing method for double-pair data dominated by the inclined pair such as in the investigated scenario, first tests using the data-driven multi-step self-de-aliasing (DMD) processing scheme (Abrykosov et al. 2022) were conducted. This processing scheme exploits the fact that the estimation of stand-alone low-degree daily solutions is possible without the data gaps of the inclined pair over the poles affecting the daily retrieval (as shown in the right panel of Fig. 14). Thereby, the correlations between the daily and multi-day solution coefficients which are present in the Wiese processing scheme can possibly be avoided. The results of these experiments will be presented in future work.

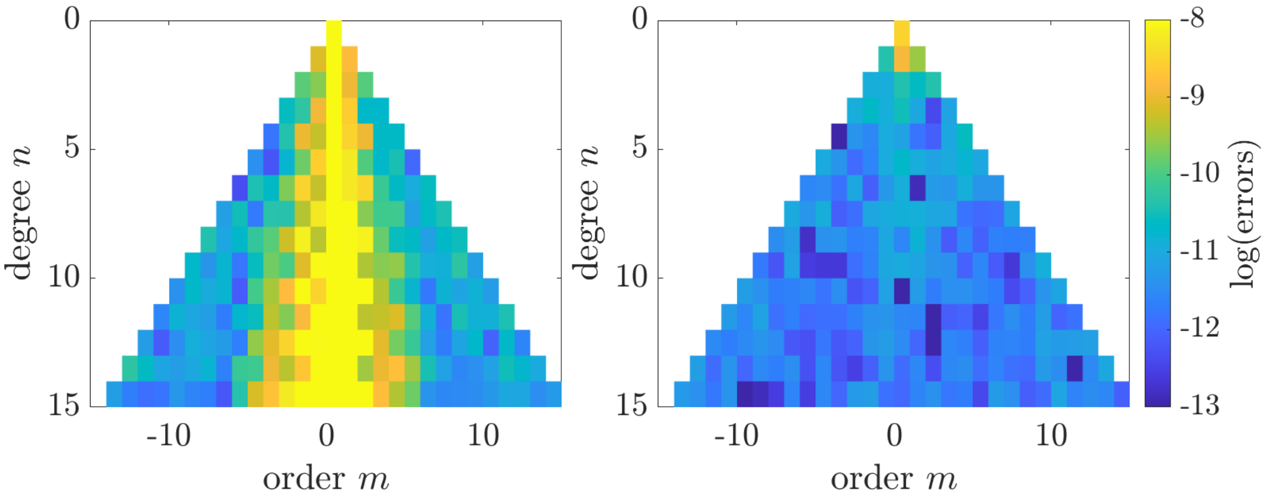

Figure 14. Left: retrieval errors of the first of the daily Wiese solutions (DWS) that have been co-estimated along with the 7-day Wiese solution shown by Fig. 11 (bottom right). Right: retrieval errors of a stand-alone d/o 15 1-day full signal and noise solution estimated based on simulated data of 1 day, for a single inclined-pair scenario based on 5d_LH orbits using NGGM-type accelerometer noise (cf. Eq. (2)) Both panels use the same colorbar.